Tectono-metamorphic evolution of the Tethyan Sedimentary Sequence (Himalayas, SE Tibet)

Accepted Manuscript

Tectono-metamorphic evolution of the Tethyan Sedimentary Sequence (Himalayas, SE Tibet)

Chiara Montomoli, Salvatore Iaccarino, Borja Antolin, Erwin Appel, Rodolfo Carosi, Istvàn Dunkl, Ding Lin, Dario Visonà

To appear in: *Italian Journal of Geosciences*

Received date: 22 July 2015

Accepted date: 09 December 2015

doi: 10.3301/IJG.2015.42

Please cite this article as:

C. Montomoli, S. Iaccarino, B. Antolin, E. Appel, R. Carosi, I. Dunkl, Ding L., D. Visonà - Tectono-metamorphic evolution of the Tethyan Sedimentary Sequence (Himalayas, SE Tibet), *Italian Journal of Geosciences* 10.3301/IJG.2015.42.

Tectono-metamorphic evolution of the Tethyan Sedimentary Sequence (Himalayas, SE Tibet)

C. Montomoli [1], S. Iaccarino [1], B. Antolin [2], E. Appel [2], R. Carosi [3], I. Dunkl [4], Ding L [5], D. Visonà[6]

1. Dipartimento di Scienze della Terra, Via S. Maria 53, 56126, Pisa (Italy)
2. Institute for Geosciences Tubingen, University of Tubingen (Germany)
3. Dipartimento di Scienze della Terra, Via Valperga Caluso 35, 10125, Torino (Italy)
4. Geoscience Center Gottingen, University of Gottingen (Germany)
5.Institute of Tibetan Plateau Research Beijing, Chinese Academy of Sciences (China)
6. Dipartimento di Geoscienze Padova, Via Gradenigo 6, 35131, Padova (Italy)

Abstract

The Tethyan Sedimentary Sequence, one of the major tectonic units of the Himalayan belt cropping out in the inner portion of the Himalayan belt, has been investigated in SE Tibet to unravel its tectonic and metamorphic evolution.

The Tethyan Sedimentary Sequence recorded at least three phases of ductile defomation, all of them associated to the development of folds and related axial plane foliations. A prominent D1 deformation is progressively overprinted by a D2 deformation approaching the Yarlung Tsangpo suture zone to the North. Structural analysis allowed to recognise two first-order different structural domains: a southern domain in which D1 is the prominent deformation and a northern domain in which the D2 overprint predominates up to transpose D1 deformation. F2 folds show a regional backward vergence (northward) with respect to the southward verging F1 folds. Finite strain data show an increase of D2-related strain moving to the North. It is worth to note that new P-T-d data on polydeformed chloritoid schists point out an increase of both temperature and pressure from D1 to D2 deformation indicating prograde burial during D1-D2 phases and support that F2 folds developed in a compressive tectonic framework during crustal thickening in the time span of 35-25 Ma. The integration of our new deformation and P-T data with available literature data will help to deconvolve the long lasted history of this tectonic unit, far away to be well understood.

Key words: Tethyan Sedimentary Sequence, SE Tibet, structural analysis, chloritoid schist

INTRODUCTION

Collisional orogens are associated to the development of folds and thrusts linked to several steps of collision leading to the development of nappe stacks with different metamorphic imprints. Folds and thrusts have respectively different facing/vergence and sense of tectonic transport depending on their structural position in the belt architecture and to the timing of their development within the frame of the whole tectonic history ranging from collisional to extensional tectonic setting. Opposite vergence is a quite common feature in many orogenic belts and double vergence orogens have been well described since a long time e.g. Alps (ARGAND 1916; SCHMIDT *et alii* 1996) and Pyrenees (CHOUKROUNE *et alii* 1990; TEIXELL, 1998).

The Himalayan belt, derived from the collision of the India and Asia plates (HODGES, 2000) is characterized by a spectacular structural continuity of the main tectonic units divided by important regional tectonic boundaries for more than 2000 km. The main tectonic transport, due to continent-continent collision is towards the S and SW and moving to the inner zone of the belt top to the north backthrusts put the Indian derived tectonic units over the Asian plate.

This work focuses on the tectonic evolution of the Tethyan Sedimentary Sequence (TSS) that is one of the main tectonic units building up the Himalayan chain. Its deformation and metamorphic history and its timing is essential to understand the evolution of the Himalayan Belt. However, the great majority of the tectono-metamorphic studies in the Himalaya focused on the medium- to high-grade metamorphic rocks of the Greater Himalayan Sequence (GHS), the tectonically lower unit, respect to TSS, in the Himalayan orogenic pile.

TSS is the northern and uppermost tectonic units made by a polydeformed package of predominantly very-low-grade to low-grade metamorphic sedimentary sequence derived from the northern Indian plate margin (GANSSER, 1964; FUCHS, 1967; BORDET *et alii*, 1971; GAETANI & GARZANTI, 1991). To the south the TSS is bounded by the South Tibetan Detachment System (BURCHFIEL *et alii,* 1992; CAROSI *et alii*, 1998), a top-down-to-the north shear zone putting the TSS in contact with the lower medium and high-grade metamorphic rocks of the Greater Himalayan Sequence (Fig. 1). To the north the TSS is separated from the Lhasa block by the Yarlung Tsangpo Suture Zone and the top-to-the-North thrust (Great Counter thrust, YIN, 2006) gets it over the melange complex of the suture zone (Fig. 1).

Although the TSS crops out for hundreds kilometres, there is a lack of a coherent regional deformation scheme and there are currently limited field-based works focusing on its deformation history and tectonic evolution (GODIN, 2003; AIKMAN *et alii*, 2008; RATCHBACHER *et alii*, 1994; ANTOLIN *et alii*, 2010, 2011). In spite of the fact that a general assessment exists regarding the oldest deformation phase linked to the first stage of continental collision an open debate exists

about the later tectonic phases, on their kinematics and genesis, especially regarding the North verging folds that have been described along several sections of the belt.

Detailed works on the tectonic evolution of the TSS have been performed in areas close to the STDS (GODIN, 2003; CAROSI *et alii*, 2002, 2007; KELLETT & GODIN, 2009; COTTLE *et alii*, 2011) focusing on the relations between the development of several generations of folds and the activity of this important tectonic discontinuity.

Aim of this work is to describe the structural and tectonic evolution and the kinematics of deformation of the TSS cropping out in a key area of the Himalayan belt, and to compare it with other significant structural sections where the tectonic unit is well represented, mainly focusing on the post-D1 tectonic evolution. Moreover, P-T estimations have been obtained on a selected key sample, showing clear (micro-) structural relationships. The integration of our new deformation and P-T data with available literature data (*e.g.* ANTOLIN *et alii*, 2011, DUNKL *et alii*, 2011), will help to unravel the long lasted history of this tectonic unit, far away to be well understood.

OVERVIEW OF THE HIMALAYAN GEOLOGY

The Himalayan belt derives from the collision of the Indian plate, to the south, and the Eurasian plate, to the north, starting from about 55-50 Ma (MOLNAR, 1984; ROWLEY, 1996, 1998; DE SIGOYER *et alii*, 2000; LEECH *et alii*, 2005; SEARLE *et alii*, 1997; SEARLE, 2001; GUILLOT *et alii*, 2003, NAJMAN *ET ALII*, 2010). During the collision the Tethyan ocean, interposed between the two plates, was completely consumed and its remnants can be now followed along the Indus-Tsangpo suture zone running from western Ladakh to south-eastern Tibet (HEIM & GANSSER, 1939; DEWEY & BIRD, 1970; FRANK *et alii*, 1977; MOLNAR & TAPPONIER, 1977; GANSSER, 1980; SEARLE, 1983; BURG & CHEN, 1984).

The major lithotectonic units are divided by a series of southwards-propagating, south verging thrusts rooting into a common basal thrust, known as the Himalayan sole Thrust (HODGES, 2000).

Moving from south to north, i.e. from the lowest to the uppermost tectonic units, we can recognize the Subhimalayan unit, made up by a Tertiary molasse (Siwalik Group) (DECELLES *et alii*, 1998), deposited in a foreland basin formed by flexural down-warping of the Indian plate beneath the Himalayan load.

The Main Boundary Thrust divides the Siwalik Group from the structurally upper Lesser Himalayan Sedimentary Sequence (LH) made by sediments deposited in a proximal position on the Indian shelf from Proterozoic to Cambrian, reaching Paleocenic ages in the more eastern sectors of the belt (STÖCKLIN, 1980; VALDIYA, 1980). The LH has been deformed by thrusts and folds under

low-to medium grade metamorphic conditions (LE FORT, 1975; PAUDEL & ARITA, 2005; DE CELLES, *et alii*, 2001; ROBINSON *et alii*, 2003).

The Main Central Thrust zone, a crustal scale top-to-the South ductile – brittle shear zone, juxtaposes the Greater Himalayan Sequence (GHS) over the LH.

The GHS consists of medium and high-grade metasedimentary and meta-igneous rocks (Le Fort, 1975, HODGES, 2000) from Neoproterozoic to Ordovician in age (HODGES, 2000), intruded in its upper portion by Miocene leucogranites (HODGES, 2000; VISONÀ *et alii*, 2012).

The GHS is divided at least into two sub-units, the lower GHS made mainly by micaschist and paragneiss, and the upper GHS made by para and orthogneiss, calcsilicates and migmatite divided by a top to the S and SW tectono-metamorphic discontinuity (MONTOMOLI *et alii*, 2013, 2015)

Two main metamorphic events affected the GHS: the first one, associated to crustal thickening, is bracketed at > 44 Ma in SE Tibet (AIKMAN *et alii*, 2008;, 2012) and from 45 to 32 Ma in Nepal (COLEMANN, 1998; Godin *et alii*, 1999; CAROSI *et alii*, 2010, 2014; IACCARINO *et alii*, 2015), while the second one occurred at 22-18 Ma during GHS exhumation and related decompressional melting (HODGES. 2002; IACCARINO *et alii*, 2015).

The South Tibetan Detachment System (STDS), a top-to-the-North brittle-ductile shear zone (BURCHFIEL *et alii*, 1992; CAROSI *et alii*, 1998) divides the GHS from the upper tectonic unit, named Tethyan Sedimentary Sequence (TSS).

TSS is a sedimentary sequence, spanning from Paleozoic to Eocene, deformed under very-low and low-grade metamorphic conditions (GARZANTI *et alii*, 1994, CROUZET *et alii*, 2007, DUNKL *et alii*, 2011). TSS is intruded by biotite-muscovite granites and leucogranites, emplaced during the Eocene-Miocene (AIKMAN *et alii*, 2008, 2012) and with their metamorphic carapaces they form the North Himalayan Gneiss Domes (NHGD) where highest metamorphic conditions have been registered (LEE *et alii*, 2000, YAN *et alii*, 2012).

To the North the TSS is bounded by the Great Counter Thrust getting it in contact with the Lhasa batholith (YIN, 2006; HARRISON *et alii*, 2000; HODGES, 2000).

TETHYAN SEDIMENTARY SEQUENCE IN SE TIBET AND GEOLOGY OF THE STUDY AREA

The study area is located in south-eastern Tibet, south of the Yarlung Tsangpo River, and it extends from Qonggyai in the west until east of Gyaca (Fig. 1). Meso and microstructural analyses have been conducted along several profiles perpendicular to the main WNW-ESE structural trend of the belt where the TSS presents superb exposures and crops out for several tens kilometres

The TSS is an almost complete sedimentary sequence deposited on the northern Indian passive continental margin and it registers the evolution of the Neo-Tethys sea, from the pre-rift stage (Cambrian – Ordovician) to the final break-up of Gondwana in early Cretaceous and subsequent sedimentation till Eocene (FUCHS, 1967; GAETANI & GARZANTI, 1991; DUPUIS *et alii*, 2006; LIU & EINSELE, 1994; GARZANTI, 1999; HODGES, 2000; YIN, 2006).

During field work we focused on the portion of the TSS constituted by a turbiditic sequence of Middle Triassic to Early Jurassic age (ANTOLIN *et alii*, 2010; 2011; CHANG 1984, MERCIER *et alii*, 1984; PAN *et alii*, 2004; WEBB *et alii*, 2013) that crops out for about 100 kilometres along the N-S study sections (Fig. 1). The flysch is made up by turbiditic sandstone, slates, black shales interbedded with sandstone and siltstone and locally some limestone (DUPUIS *et alii,* 2006; DUNKL *et alii*, 2011). The sequence is intruded by Cretaceous mafic dikes and contains also some ultramafic bodies (ZHU *et alii*, 2008; XU *et alii*, 2009; DUNKL *et alii*, 2011).

To the north the TSS is delimited from a mélange complex and the Cretaceous clastic rocks by the top-to-the North Renbu-Zedong thrust (YIN *et alii*, 1994, 1999) and correlated with the Great Counter Thrust cropping out westward (YIN *et alii*, 1994; HARRISON *et alii*, 2000) active between 19 and 15 Ma (QUIDELLEUR *et alii*, 1997; LI *et alii*, 2015). The mélange complex (constituted by cherts, shales, marbles, andesite, diorites, mafic and ultramafic bodies, limestones and phyllite) has been deposited on the growing Neo-Tethys ocean floor and incorporated in a subduction complex mélange (SEARLE *et alii* 1987). The Cretaceous clastic rocks were deposited in the active palaeomargin of the Indus Yarlung Suture Zone (HARRISON *et alii*, 2000; PAN *et alii*, 2004; DUPUIS *et alii,* 2005).

The southward dipping Renbu–Zedong thrust has been dated from 19 to 11 Ma (QUIDELLEUR *et alii*, 1997).

To the south the Triassic flysch is limited by the north dipping Lhunze fault (Fig.1), that divides it from the Jurassic and Cretaceous portion of the TSS sequence (PAN *et alii*, 2004). The Lhunze fault has been correlated with the Gyrong-Kangmar thrust, mapped 200 km westward (AIKMAN *et alii*, 2008)

AIKMAN *et alii* (2008) recognized in the study area a polyphase tectonic history. E-W trending south-verging folds, due to N-S shortening event, have been later reoriented by the Great Counter Thrust giving rise to North verging back-folds. The subsequent tectonic evolution is linked to East-West extension with the development of North-South trending graben (AIKMAN *et alii*, 2008; ANTOLIN *et alii*, 2010).

Close to our investigated area, near Kangmar, in a zone located between Gyantze and Lhaze, RATCHBACHER *et alii* (1994) distinguished syn- and post-collisional structures. The sin-collisional

ones are represented by F1 southverging folds, while the second ones are represented by faults and top-to-the South foreland-directed thrusts and backthrusts and minor upright folds. While the sin-collisional structures are widely spread, the post-collisional ones are concentrated, according to RATCHBACHER *et alii*, (1994), only close to the suture zone.

In the study area the TSS has been intruded by Eocene-Oligocene granitoids (Yala Xiangbo Dome and Dala granitoids) (AIKMAN *et alii*, 2008, 2012; ZHANG *et alii*, 2005, 2012; Hou *et alii*, 2012; Zeng *et alii*, 2011).

STRUCTURAL DATA

Meso- and microscopic structural analysis has been performed along several sections perpendicular to the trend of the belt (Fig. 1). Field and microstructural data point out the presence of three main ductile deformation phases.

The study area has been divided into two structural domains based on the dominant phase of deformation and related fabric orientation (Fig. 1). The first structural domain is characterized by the predominant development of D1 deformation phase, and it is located southward of the Yala Xiangbo dome (Fig. 1). The second structural domain is more to the north and it is characterized by the predominant development of the D2 tectonic phase (Fig. 1).

1 - D1 tectonic phase

D1 phase is very well expressed in the southern sector of the study area (Fig.1) and it is characterized by the occurrence of metric to decametric F1 folds. Their geometry can be referred mainly to classes 1B (parallel folds), 1C and subordinately to class 2 (similar folds) according to Ramsay's classification (RAMSAY, 1967).

Best examples have been observed south of Qonggyai where F1 folds reach decametric size. Well-preserved sedimentary structures, such as graded bedding and load structures, led to determine the southward facing of F1 folds (Fig. 2a).

F1 axial planes are from moderately to steeply dipping toward the north pointing out a southward vergence of F1 folds. A1 axes trend between ENE-WSW and plunge a few degrees both to the NE and to the SW (Fig. 1).

On F1 fold limbs extensional fibrous composite veins (made by quartz and calcite fibres), from millimetres to centimetres in size, have been observed. Veins are confined in the more competent levels and they can be related to the beginning of boudinage processes during folding. Fibres in veins are oriented parallel to the stylolitic foliation plane and perpendicular to A1 fold axes. Along folds profiles bedding parallel calcitic veins have been detected too. They developed at

the beginning of shortening when fluids were channelized between bedding interfaces along the clay layers.

Parallel to F1 axial plane a penetrative S1 foliation has been observed (Fig. 2a). S1 strikes mainly WNW-ESE and dips predominantly towards the NE. The development of S1 foliation is strongly influenced by rock composition and competency and it shows different aspects in different sampled areas.

On S1 surfaces object lineations (*sensu* PASSCHIER & TROUW, 2005) are represented by mineral lineations made by quartz and calcitic fibres around rigid objects. Best examples are represented by fibres grown around pyrite crystals that in some cases reach centimetric size. Fibres mainly strike NW-SE (Fig. 2b).

1.1 - Microstructures and deformation mechanisms.

To the South, at the microscopic scale, S1 varies from a stylolitic foliation to a fine continuous foliation. In the first case pressure solution is the dominant deformation mechanism and no dynamic recrystallization has been observed along dissolution planes. Pressure solution mechanisms are highlighted by the presence of dark stylolitic surfaces along which undissolved material is concentrated and by the abundance of truncated detrital quartz grains.

A weak dynamic recrystallization along S1 foliation surfaces and in strain fringes around porphyroclasts have been observed when S1 becomes a fine continuous foliation (Fig. 3a). Synkinematic recrystallization is represented by white mica, chlorite, quartz, calcite and opaques.

Moving to the North, dynamic recrystallization increases, and S1 becomes a well expressed fine continuous foliation in the more pelitic layers and an anastomosing spaced foliation in more arenitic ones. Detrital quartz crystals show evidence of undulose extinction.

Fibres around pyrite crystals, defining object lineations, are of pyrite type (RAMSAY, 1980) and at the microscale both face and displacement controlled types occur (DURNEY & RAMSAY, 1973).

Calcite crystals of bedding parallel veins registered syntectonic twinning that are mostly referable to type II (BURKHARD, 1993), and only in very few cases Type I and Type III have been observed, pointing out to deformation temperatures between 200 and 300°C in accordance also with undulose extinction observed on quartz grains.

2 - D2 tectonic phase

D2 tectonic phase overprints older D1 structures and it can be detected all over the study outcrops with different characteristics and strain intensity.

In the southernmost outcrops D2 tectonic phase is detectable just by the presence of millimetric to centimetric F2 folds whereas, moving to the North, F2 folds are better developed reaching metric size. F2 folds have mostly southward dipping axial planes supporting a northward vergence i.e. opposite to F1 folds vergence, even if in the more southern areas it dips to the north (Fig. 2c).

According to Ramsay's classification F2 can be ascribed mainly to classes 1B (parallel) and 2 (similar). They show different opening angles varying from 25° to 85°. A general decrease of opening angle values can be observed moving from South to North.

A2 axes and intersection lineations (between S1 and S2 surfaces) trend NW-SE and plunge both toward the SE and the NW (Fig. 1).

Parallel to F2 axial planes an S2 foliation has been recognized. S2 strikes E-W with variable dipping values both towards the North (southern areas) and to the South (northern areas). S2 is a crenulation cleavage in the more southern areas, while moving to the North it becomes a fine continuous foliation.

In the northern sector of the study area, approaching the suture zone several brittle-ductile shear zones have been detected (Fig. 2d). In the southernmost outcrops they have been observed they are localized on the overturned limbs of F2 folds. Overprinting criteria point out that shear zones developed during the late stages of D2 tectonic event. Moving to the north, i.e. approaching the suture zone, the shear zones completely transpose F2 structures.

When the shear zones are located on the overturned limbs of F2 folds they are centimetric in thickness, while they reach metric thickness when they completely transpose the folds.

Kinematic indicators are mainly represented by C-S fabric (BERTHÈ *et alii*, 1979), deflection of the main foliation and minor drag folds (Fig. 2d). C surfaces strike mainly N080, 20S while S surfaces are N110, 45S. Stretching lineations trend N170 and dip e few degrees towards the South (Fig. 1). Kinematic indicators point out a top-to-the-North sense of shear (Fig. 2d).

2.1 -Microstructures and deformation mechanisms.

Moving from South to North S2 is increasingly well developed and primary structures are no longer detectable.

In the southern areas S2 is a discrete crenulation cleavage and it is not associated to synkinematic recrystallization (Fig. 3a). Moving to the north a gradual transition to a fine continuous foliation can be followed (Fig. 3b). S2 develops as a fine continuous foliation in narrow

zones whose thickness varies from few centimetres to decimetres. Moving to the North S2 becomes the main surface at the outcrop and it completely transposes the S1 foliation. In the northernmost outcrops it can be classified as a fine continuous foliation associated to a dynamic recrystallization represented by white mica, chlorite, quartz, calcite and oxides (Fig. 3c).

It is worth to note that moving from South to North, the spacing among S2 foliation domains (*sensu* PASSCHIER & TROUW, 2005) changes. An estimation of the spacing of foliation domains has been attempted at the microscale comparing the same lithotypes, i.e. pelitic arenites predominant in the Triassic flysch. The spacing between foliation domains decreases moving from south to north and, at the same time, the thickness of foliation domains grows up.

Deformation mechanisms are mainly represented by ductile deformation of quartz crystals with evidences of undulose extinction. Ductile deformation has been recognized also in calcite crystals in shear veins developed parallel to shear zone boundaries. The calcite crystals show e-twin lamellae (BURKHARD, 1993). The thickness of a single lamella is, usually greater than 1 mm. In some cases the twins are gently bended mainly along the external border. These features are consistent with the types II and III defined by BURKHARDT (1993) confining deformation temperature range between 200 and 300°C.

2.2 - Finite strain analyses

Measurements of finite strain have been performed on fold profiles and on selected samples from metarenites levels of the Triassic flysch in order to constrain strain partitioning during the D2 tectonic event. We estimated the finite strain along a S-N section in relation to the D2 tectonic events following Lisle's method (LISLE, 1992). We analyzed F2 folds that show no evidence of flexural slip deformation mechanism and which are not affected by later F3 folds.

The Lisle's method is based on the geometrical analyses of folds, measuring the orthogonal thickness of folded layers (t) at different dips of the limbs (a). The method's basic assumption is that, at the beginning of fold development, buckling is the main acting mechanism and folds firstly developed with a constant thickness around their profile. With subsequent increasing of deformation folds profiles are modified becoming more and more flattened so that thinning along their limbs and thickening in the hinge zones are registered. Following Ramsay's classification (1967) the progressive strain results in the transformation of class 1B folds into class 1C folds.

If deformation is homogeneous, after flattening, the folds profiles are modified so that the orthogonal thickness of the layer at any point, around fold profile, is inversely proportional to the stretch. In such a way it is possible to directly construct the strain ellipse plotting in a graph, in

polar co-ordinates, the inverse of the thickness (*1/t*) as a function of orientation of the layer tangent (*a*). The strain ellipse is fitted through the points on the inverse thickness graph.

We measured the orthogonal thickness of layers in sections perpendicular to the fold axes so the estimated ellipse axial ratio corresponds approximately to the XZ plane of finite strain ellipsoid (Fig. 4)

Strain ratio values are shown in Table 1 and they point out an increase moving from the southernmost outcrops to the northernmost ones, approaching to the Great Counter thrust. Strain values vary between 4.4 (northernmost analised F2 fold) and 1.27 (southernmost outcrops).

Finite strain analyses have been performed also on selected metarenite samples coming from the same N-S transect applying both Fry and Ramsay methods (FRY, 1979; RAMSAY, 1967) on section parallel to XZ plane of finite strain ellipsoid. Samples have been cut parallel to mineral lineation and perpendicular to S2 foliation.

Basic assumptions for the Fry method to get good results are that the distribution of markers has to be homogeneous and isotropic (see GENIER & EPARD, 2007 for a critical review). We used detrital quartz grains as strain markers that are quite homogeneously distributed in the samples and size distribution of particles are well sorted so that we obtain good regular vacancy fields surrounded by a higher density corona in the Fry diagrams (Fig.5).

Fry's method has been applied using EllipseFit 3.2.0. program (VOLLMER, 2015) on six samples and from 91 to 282 centers have been considered.

R_{XZ} values vary from 1.23 to 1.48 (Table1) moving from South to North showing an increase along the sampled section.

On the same samples, applying Ramsay's method (1967), we obtained the same finite strain increasing trend and R_{XZ} values vary from 2.07 to 2.66 moving along the same S-N direction (Table 1).

The second applied method shows generally higher values than the first one. This could be probably due to the fact that the R_{XZ} values measured are the results of two superimposed tectonic events (D1 and D2) so that the elliptical shape of quartz grains could be acquired during the polyphase tectonic history, i.e. during D1 and D2. Fry's method could be the best one because it is not dependent on the shape of the strain makers, but it is just a function of particle centers distribution. In both cases an increase in deformation has been observed moving from the south to north, approaching to the suture zone.

3 – D3 tectonic phase

This tectonic phase is not ubiquitously developed in the study area. It is associated to the development of decametric upright folds deforming all the previous structures. Folds are characterized by rounded hinges and quite wide opening angle. F3 fold axes trend E-W.

The S3 axial plane foliation is a crenulation cleavage (Fig. 3d). No dynamic recrystallization has been observed along S3 foliation.

METAMORPHIC DATA

1- Overview of metamorphism in the TSS

The Tethyan Sedimentary Sequence experienced, generally, very-low to low-grade metamorphic conditions during deformation (GARZANTI *et alii*. 1994; HODGES, 2000; CROUZET *et alii*, 2007; AIKMAN *et alii*, 2008; DUNKL *et alii*, 2011). Several applied methods such us: illite crystallinity (GARZANTI *et alii*, 1994, CROUZET *et alii*, 2007), RSCM thermometry (COTTLE *et alii*, 2011; KELLETT & GRUJIC, 2012) and classical thermometry (CROUZEt *et alii*, 2007) estimated peak palaeo-temperatures from 250°C to 450°C. In the study area DUNKL *et alii* (2011) through illite and chlorite cristallinity obtained diagenetic to high anchizone-low epizone conditions for D1 tectonic phase, whereas middle epizone conditions were determined for the D2 tectonic event. Beside, DUNKL *et alii* (2011) in the study area, determined higher metamorphic conditions, for two samples (WE-12 and SR-21a of DUNKL *et alii*, 2011) for which they determine P of about 7.8 Kbar and T around 600°C respectively.

Higher metamorphic conditions have been detected for the lower portion of the TSS, that discontinuously crops out along the belt reaching amphibolite facies conditions (JESSUP *et alii*, 2008; CORRIE *et alii*, 2012, CAROSI *et alii*, 2013).

In order to carry a contribution towards the understanding of tectono-metamorphic evolution of TSS, in this work we studied a chloritoid - bearing schist sample (WE-09 in Fig. 1).

2 –Samples petrography and microstructures

WE-09 sample has a porphyroblastic texture with large (up to 1 mm in length) chloritoid porphyroblast, whereas micas have a finer grain size (Fig. 6a-b). The sample has a paragenesis made of chloritoid + white mica + chlorite + quartz + rutile (Cld + Wm + Chl + Qz + Rt following mineral abbreviations after WHITNEY & EVANS, 2010 except for Wm), whereas zircon, tourmaline, minor allanite and (detrital?) monazite (Zrn, Tur, Aln, Mnz abbreviations after WHITNEY & EVANS, 2010) have been detected as accessories phases. Cld grains are optically zoned, with an inclusions (tiny Wm, Qz, Chl and Rt) rich greenish core and pale-green inclusion-poor rim (Fig. 6a-b-d).

WE-09 sample registered the three ductile described tectonic phases and S1, S2 and S3 foliations can be recognized (Fig. 6). The earlier foliation (S1), is a continuous slaty cleavage defined by GSPO (*i.e.* Grain Shape Preferred Orientation, PASSCHIER & TROUW, 2005) of synkinematic Wm, Chl, ±Cld, preserved within the microlithons of the S2 foliation, that could be classified as a crenulation cleavage defined by GSPO of synkinematic Wm, Chl and Cld (Fig. 6a-b). The late foliation, S3, is a smooth and wider spaced (with respect to S2) crenulation cleavage oriented at high angle respect to the S2 (Fig 6d). S3 is defined by insoluble material and rarely by re-orientation of former mica grains. Cld shows a quite complex blastesis-deformation relationships respect to the deformation picture described above (Fig. 6a-d). Cld dissolution along S3 planes (Fig. 6d) testifies how Cld is a pre-D3 mineral, whereas relationship with D1-D2 are much more complex. Cld oriented at high angle respect to S2 with its internal foliation (Si) discordant with the main external one (S2), strain caps and Qz pressure shadows around Cld testifies how its growth occurred in the late stages of D1 deformation event (Fig. 6a). On the contrary, some Cld crystals show a nearly continuous internal foliation Si with the external S2 supporting that part of Cld growth is synkinematic with respect to the development of S2 (Fig. 6d). Sporadic decussate chloritoid overgrowing S2 is also observed (Fig. 6c). These observations together support a continuous growth of this mineral from late D1 phase up to late/post D2 phase and before D3 phase.

3 - Mineral chemistry

Mineral phases have been qualitative identified with EDS system during SEM work at University of Turin, where also X-ray element maps on Cld were acquired. After, the main silicate minerals (Cld, Wm and Chl) were quantitative chemically characterized at the Dipartimento di Geoscienze (Università di Padova) with a CAMECA SX50 Electron Microprobe (EMP), using the analytical protocol reported in CAROSI *et alii* (2010). Multiple points and grain traverses have been obtained in order to cover the whole texturally different minerals. Mineral structural formulae were calculated with the A-X software obtained from Tim Holland personal webpage (http://www.esc.cam.ac.uk/research/research-groups/holland/ax).

Chloritoid porphyroblast could be classified as "Fe-rich" Cld (Tab.2) as defined in POURTEAU *et alii*, 2014. Al_{tot} p.f.u. ranges from 1.97 to 2.01, whereas Fe^{3+} p.f.u. is < 0.01 (Tab.2). Cld shows a clear zoning from core to rim in major elements with a progressive increase of XMg ($Mg/(Mg+Fe^{2+})$) from *c.* 0.12 up to nearly 0.18 also coupled with a reduction of manganese (Fig. 7a).

White mica is a celadonite-poor muscovite with a clear interlayer cations deficit (K+Na+Ca<0.91) that may be due to some substitution of the pyrophyllite end member (*e.g.* WILLNER *et alii*, 2009). Si^{4+} p.f.u. ranges from 3.02 up to 3.16 (Tab.2, Fig. 7b) and a correlation between Wm composition and microstructural position is also suggested, indeed S1 Wm have generally a lower Si^{4+} p.f.u. content respect to S2 Wm (3.02-3.10 vs 3.07-3.16 p.f.u., respectively). XPg (Na/(Na+K) is in the range of 0.12-0.20.

Chlorite is characterized by a quite homogeneous composition with XMg in the range of 0.44–0.50 and Si p.f.u. varies between 2.97-3.07. No clear correlation is present among Chl microstructural position and its chemistry.

4 - P-T estimates

4.1- Methodology

Constrains on the P-T history of sample WE-09 was obtained either with P-T pseudosections approach either with empirical chloritoid-chlorite Fe-Mg exchange, pressure independent, empirical thermometer of VIDAL *et alii* (1999). A P-T pseudosection in the ten components, MnO-Na_2O-CaO-K_2O-FeO-MgO-Al_2O_3-SiO_2-H_2O-TiO_2 (MnNCKFMASHT) model chemical system, was constructed with the software Perple_X (CONNOLLY, 2005) in the P-T range of 0.05-1.05 GPa & 350-600 °C. Iron was assumed as ferrous, since: *(i)* low amount of ferric iron in mineral formulae was estimated with the A-X software and *(ii)* the presence of Rt (as inclusion and matrix mineral) and the lack of Mag should indicate low oxidation conditions (*e.g.* LO PÒ & BRAGA, 2014). Calculations were performed with the thermodynamic data set of HOLLAND & POWELL (1998, with the 2002 upgrade) and with the CORK fluid equation of state (HOLLAND & POWELL, 1991). Solid solution models used in the calculations were: TiBio(HP) for biotite, Pheng(HP) for potassic white mica, Ctd(HP) for chloritoid, Chl(HP) for chlorite, Gt(HP) for garnet, IlGkPy for ilmenite, Carp for carpholite, St(HP) for staurolite, hCrd for cordierite, T for talc (further details on solution models see http://www.perplex.ethz.ch/perplex_solution_model_glossary.html). The models used for feldspars (plagioclase and K-feldspar) and paragonitic mica were reported by MASSONNE (2012 and references therein). Raw graphical results were manually redrawn as shown in CONNOLLY (2005).

Bulk rock composition was obtained, on thin section chip, by X-ray fluorescence spectroscopy (XRF) analysis using WDS sequential Philips PW2400 spectrometer, hosted at Dipartimento di Geoscienze (Università di Padova) equipped with a 3 kW Rh X-ray tube, 4 filters (Al 200 μm, Brass 100 μm, Pb 1000 μm and Brass 300 μm), 3 collimators (150 μm, 300 μm and 700 μm), 5 analyzing crystals (LiF220, LiF200, Ge111, PE002, TlAP100), 2 detectors (flow counter and scintillator), and the sample changer Philips PW2510 with 30 sample holders. The analyses,

performed under vacuum conditions, and using the SuperQ software from Panalytical, were based on calibrations calculated on geological reference standards (GOVINDARAJU, 1994).

4.2 - P-T results

Sample WE-09 bulk composition plots in the high-Al pelite field of AFM diagram according to SPEAR (1993), whereas in the HERRON (1988) classification it falls in the shale field.

The WE-09 P-T pseudosection is presented in Fig. 8a. Cld is predicted to be stable in a very large part of the calculated P-T space, except in the HT side (timbered part of Fig. 8a) where Cld is no more stable (*e.g.* consumed to produce St).

The observed WE-09 phase assemblage (in bold in Fig. 8a) occupies a large part of the P-T range and it is limited by the occurrence of garnet, ilmenite, plagioclase, epidote and staurolite (Fig. 8a, Fig.9), not observed in the sample. Small modal amount (<5%) of Pg is predicted to be stable in the P-T field, even if was not observed, and it could be reasonably inferred to occur in submicroscopic interlayers in white mica (*e.g.* WILLNER *et alii*, 2009; POURTEAU *et alii*, 2014).

Relevant isopleths are shown in Fig. 8b,c. XMg isopleths in Cld have an almost always sub-vertical shape and are largely function of the T. Si p.f.u. isopleths in potassic white mica (Fig. 8b) have a nearly flat slope and increase with rising pressure.

According to isopleths contouring (*i.e.* XMg Cld, Fig. 8c) the observed Cld zoning (XMg core=0.118-0.122, XMg rim=0.167-0.177) testifies a prograde T increase from c. 425-450°C up to 500-550°C.

T estimates, with empirical calibration of VIDAL *et alii* (1999) for chloritoid rim (XMg rim=0.167-0.177) matched with matrix chlorite (XMg= 0.48-0.50) gives T in the range of 494-541 °C (±60°C, VIDAL *et alii*, 1999). Coupling Cld rims with matrix chlorite with lowest XMg (0.44), gives still higher temperature 571-599°C, which appears too much high if compared with mineral assemblage predicted by P-T pseudosection at the same temperature (Cld absent fields, Fig. 8), and it could indicate non-equilibrium condition among these selected mineral pairs (*e.g.* FRANCESCHELLI & MEMMI, 1999). The lack of suitable chlorite grains in the core of the chloritoid prevents a strictly constrained application of this thermometer for the chloritoid core. If we assume that Cld core (XMg=0.118-0.122) was in equilibrium with matrix chlorite with the lowest XMg (*i.e.* XMg=0.44) temperature values 0f 448-458°C (±60°C, VIDAL *et alii*, 1999) are obtained, in good agreement with pseudosection estimates. If Cld core is coupled with Chl with the highest XMg (0.50) still lower T, in the range of 390-398°C, are obtained. Despite VIDAL *et alii* (1999) cautioned to use this empirical thermometer for extreme rich Fe- and Mg- composition, we observe a good overlap between this thermometer and P-T pseudosection results and in both cases core to rim estimates

(see also LO PÒ & BRAGA, 2014), testifies a prograde growth of Cld. Indications on pressure change could be obtained with Wm chemistry. Lower Si^{4+} (p.f.u.) observed on Wm on the S1 (see above), indicates a P of equilibration of nearly 0.35-0.55. Wm on S2 show higher Si (with an average of 3.11 p.f.u.) and they indicate equilibration of the rock at a peak pressure of nearly 0.75–0.85 GPa.

These chemical pattern (Cld zoning and Wm heterogeneity) coupled with microstructural observations suggest that WE-09 sample experienced an increase of P during the prograde growth of Cld reaching "P-T-peak conditions" of *c.* 0.75–0.85 GPa, 500-525°C.
In this way a "clockwise" P-T path is reconstructed in the WE-09 sample (Fig. 9), where a T as well P increase occurred from D1 to D2 stages. The lack of Ilm, Pl, Grt and St production on cooling, permits to exclude substantial heating on decompression (Fig. 9) of the P-T path segment after metamorphic peak (red dashed line in Fig. 9), likely related to D3 event.

DISCUSSION

Meso- and microstructural analyses highlighted the presence in the study area of three main ductile events followed by a brittle phase of deformation. The first D1 deformation phase is linked to the development of south-facing E-W trending F1 folds with associated a very-low grade axial plane foliation. The D2 tectonic phase is heterogeneous and it is associated to E-W trending F2 folds, from upright to North-verging, associated to an axial plane foliation. During the late stages of D2 tectonic event top-to-the north brittle-ductile shear zones developed.

A further D3 tectonic phase, not ubiquitously developed, gives rise to hectometric upright open folds. Later NE-SW normal faults cut the sequence developing the Yadong Gulu rift (RATSCHBACHER *et alii,* 1994; ANTOLIN *et alii*, 2010).

Structural analysis allowed to individuate in the study area two main structural domains: a southern domain where the D1 ductile event predominates and a northern domain where the D2 ductile event is the main one and S2 is the main structural surface at the mesoscale.

All along the chain a polyphase tectonic history of the TSS has been already recognized by previous studies (BURG & CHEN, 1984; COLCHEN *et alii*, 1986; BROWN & NAZARCHUK, 1993; RATCHBACHER *et alii*, 1994; GODIN, 2003; GODIN *et alii*, 1999; VANNAY & STECK, 1995; WIESMAYR & GRASEMANN, 2002; CAROSI *et alii*, 2002 and 2007; ARMIJO *et alii*, 1986; MURPHY & YIN 2003; AIKMANN *et alii*, 2008) and most of the Authors agree that the principal deformation phase D1 is related to Tertiary shortening and led to the development of widespread south verging folds during a compressional tectonic setting. Geochronological data for D1 deformation phase are

around 50 Ma (RATCHBACHER *et alii*, 1994) and ~ 45 Ma (GODIN, 2003; KELLET & GODIN , 2009; DUNKL *et alii*, 2011)

A minor amount of data is available for the post-D1 tectonic evolution and there is a not a general agreement on the tectonic interpretation and kinematics of the later folding events.

In addition most of the studies about the D2 tectonic phase are concentrated close to the South Tibetan Detachment (KELLETT & GODIN, 2009; CAROSI *et alii*, 2002 and 2007). Detailed structural analyses have been performed in central and western Nepal. In central Nepal (Annapurna Range), some Authors (GODIN *et alii*, 1999; GODIN, 2003; KELLETT & GODIN, 2009; GODIN *et alii*, 2011) agree that the D2 deformation phase associated to North-verging F2 folds developed in a compressive tectonic setting (D2 of GODIN, 2003) and pre-dates the activity of the STDS (D3 tectonic phase of GODIN, 2003).

A different interpretation has been proposed by CAROSI *et alii* (2002 and 2007) which interpreted, in western Nepal, the north-verging F2 folds coeval with the activity of the STDS developed in an extensional tectonic setting. A recent reinterpretation in the Annapurna range by SEARLE (2010) confirms the extensional tectonic setting for the F2 folds.

Structural studies closer to our investigated area (RATSCHBACHER *et alii*, 1994) distinguished a post collisional deformation event, whose main effect is the reactivation of the suture zone along which most of the deformation is concentrated.

Post-collisional deformations are represented by several fault sets and by top-to-the south foreland-directed thrusts and backthrusts. Also minor folds, from open to tight, generally upright are associated to the post-collisional event. Most of post-collisional structures are concentrated along the boundaries of tectono-stratigraphic units between the Gandgese belt in the north and the TSS, i.e. Indian shelf, in the South. Backthrusts mainly developed in the Xigaze group cropping out in between the TSS and the Gandgese batholith.

Post-collisional deformations are not widespread in the TSS and develop only very close to the Suture zone deforming previous sin collisional structure.

In the study area, AIKMAN *et alii* (2008) described north-verging folds interpreted as the result of a passive reorientation of older south-verging F1 folds due to the activity of the Great Counter Thrust towards the North. So they assess that the recognized north verging folds are not due to an additional folding phase, but F2 structures are just due to a local reorientation of F1 axial planes.

Data collected during this work are in agreement with previous Authors regarding the oldest D1 tectonic phase and the youngest tectonic phase linked to E-W extension, but some main points

have to be discussed regarding the D2 tectonic event, as our data point out a much more complex evolution for this deformation phase.

Meso and microstructural analyses highlighted that D2 did not developed only close to the suture zone (RATSCHBACHER *et alii*, 1994) but it is widespread all over the study area and it can be recognized at least 100 kilometres southward of the suture zone itself.

D2 has a marked heterogeneous development. In the southern structural domain it is associated to the development of a crenulation cleavage and only centimetric minor folds can be observed. Moving towards the North (northern structural domain) F2 folds developed from metric to decametric scale and from upright they become overturned approaching the suture zone. S2 foliation, moving northward, becomes progressively much better defined and it is also associated to dynamic recrystallization. S2 transposes completely the older S1 foliation, becoming the main structural surface in the field.

Our data suggest that the northward vergence of F2 folds is not an apparent one (AIKMAN *et alii*, 2008) and it is not due to a local reorientation of F1 axial planes due to the activity of STD-MCT fault system (AIKMAN *et alii*, 2008); on the basis of meso and microstructural data (clear development of S2 foliation parallel to F2 axial planes and folding of S1 foliation in the hinge zones of F2 folds) we can asses that D2 is a distinct tectonic phase linked to a N-S shortening event.

The end of D2 tectonic event in the study area has been dated, in the Northern structural domain, at about 24-22 Ma (DUNKL *et alii*, 2011) predating the STDS activity. The STDS closer to the study area crops out southward in Bhutan several tens kilometres southwards. Th/Pb geochronology dating in granites belonging to its footwall indicates that it was active at 12.5-12 Ma and 15.5-11.0 Ma in the Khula Kangri Massif and the Masang Kang area respectively (EDWARDS & HARRISON, 1997; WU *et alii*, 1998). KELLETT *et alii* (2009) through U-Pb geochronology of magmatic zircons in deformed leucogranites and sills give ages between 15.5 and 10 Ma. A strand of the STDS cropping out a little bit westward, in Sikkim, has been dated through zircon and monazite at ca. 17 and 15-14 Ma (CATLOS *et alii*, 2004).

This can be in agreement with what has been proposed for the F2 folds in central Nepal. Here GODIN *et alii* (1999, 2011), GODIN (2003) and KELLETT & GODIN (2009) proposed that F2 folds may have originated during an Oligocene contractional event before the ductile motion of the Annapurna detachment (i.e. STDS in Kali Gandaki area, central Nepal) on the basis of crosscutting relationships, geometric and kinematic constraints and U-Pb geochronology.

By the way an open question regards the relations among the TSS deformation events and granitoids emplacements. AIKMANN *et alii* (2008) report that the Eocene granitoids (Dala granitoid) emplaced after the D2 deformation, placing an older lower bound to the D2 tectonic phase. By the

way this supported that a significant crustal thickening should have been occurred during the first tectonic phases of Himalayan orogenesis, according to the Authors during the first 10-20 Ma (AIKMANN *et alii*, 2008).

Our metamorphic data indicate prograde burial during D1-D2 phases (Fig. 9) and support that F2 folds developed in a compressive tectonic framework during crustal thickening. Moreover, our "peak" estimates for the study sample, are in good agreement with previous estimates of "relatively" close WE-12 sample (meta-mafic dyke) in DUNKL *et alii*, 2011, which reported equilibration T-P values of 474±35°C (or better ±50°C, see DUNKL *et alii*, 2011) and 0.64 (± 0.16 GPa) and with SR-12a sample (531±13°C and 0.94±0.1 GPa). The present metamorphic findings are further evidences that *"the multiple folded thrust pile of TSS"* has experienced thermal peak conditions up to amphibolite facies (DUNKL *et alii*, 2011). These medium-grade TSS rocks are preserved, beside to near the STDS and to the NHGD, also in some localities (as for instance WE-09, SR 12a localities) where sufficient structural thickening related to thrust imbrications and large scale folding is observed (e.g. HODGES, 2000).

Older ages for D2 tectonic phase have been proposed by CROUZET *et alii* (2007) that found, in western Nepal, K/Ar ages around 30-25 Ma. Moreover secondary pyrrhotite remanences support that F2 folding, in the same area, was about 35-32 Ma (APPEL *et alii*, 1991, 2012; CROUZET *et alii,* 2001; SCHILL *et alii*, 2003).

In the northernmost sectors of the study area, i.e. close to the suture zone, brittle – ductile shear zones developed always showing a top-to-the-North sense of movement. The shear zones developed on the reversed limb of F2 north-verging folds but moving closer to the GCT and to the SZ they become wider and completely transpose F2 folds. Overprinting criteria between shear zone and F2 folds led us to conclude that shear zone developed during or after the last stages of D2 deformation. Their sense of tectonic movement and the strengthening of non coaxial deformation approaching the suture zone led us to correlate them with the GCT activity constrained between 18-10 Ma bringing the TSS over the Gangdese belt of the Lhasa block (Fig. 1).

CONCLUSIONS

In this contribution we present meso and microstructural data to better constrain the tectono-metamorphic evolution of TSS in Southern Tibet. Structural and tectonic evolution of the TSS is still poorly constrained due to the lacking of data and difficult access in Tibet.

- The TSS in the study area registered at least three ductile defomation phases all of them associated to the development of folds and related axial plane foliations;

- two different structural domains have been recognized: a southern domain in which D1 is the prominent deformation and a northern domain in which the D2 overprint predominates;
- D2 shows a backward vergence (northward) with respect to the D1 tectonic phase;
the northward vergence of F2 folds is not a local phenomena, related to the activity of the STDS, but it is regionally developed
- D2 –related deformation is progressively more penetrative approaching the suture zone;
- finite strain analyses on F2 folds and on selected samples show a strain increase from South to North for the D2 tectonic phase;
- in this work we confirm a T increase from D1 to D2 along a continuous nearly N-S section and for the first time we highlight a pressure increase from D1 to D2 tectonic phases.
Anyway, further investigations are necessary to better understand the relationships among earlier deformation event and magmatism in the inner portion of the TSS.

Acknowledgments
Financial support from DFG under the priority programme SPP 1372 "Tibetan Plateau: Formation, Climate, Ecosystems" (TiP) (E. Appel), Prin 2010-2011 (C. Montomoli and R. Carosi) and PRA_2016_40 (C. Montomoli). We thank Dott. P. Mosca and Prof. J.L. Epard for their critical reviews of the manuscript improving its quality.

REFERENCES

Argand E. (1916) – Sur l'arc des Alpes occidentales. Eclogae Geologicae Helvetiae, 14, 145–191.

Aikman A.B., Harrison T.M. & Lin D. (2008) - Evidence for Early (>44 Ma) Himalayan Crustal Thickening, Tethyan Himalaya, southeastern Tibet. Earth and Planetary Science Letters, 274, 14-23.

Aikman A.B., Harrison T.M. & Herman J. (2012) - Age and thermal history of Eo- and Neohimalayan granitoids, Eastern Himalaya. Journal of Asian Earth Sciences, 51, 85–97.

Antolín B., Appel A., Gloaguen R., Dunkl I., Ding L., Montomoli C., Liebke U. & Xu, Q. (2010) - Paleomagnetic evidence for clockwise rotation and tilting in the eastern Tethyan Himalaya (SE Tibet): Implications for the Miocene tectonic evolution of the NE Himalaya. Tectonophysics, 493, 172-186.

Antolín B., Appel A., Montomoli C., Dunkl I., Ding L., Gloaguen R. & El Bay R. (2011) - Kinematic evolution of the eastern Tethyan Himalaya: constraints from magnetic fabric and

structural properties of the Triassic flysch in SE Tibet. In: Poblet, J., Lisle, R. (Eds.), Kinematic Evolution and Structural Styles of Fold-and-Thrust Belts: Geological Society of London Special Publications, 349, 99-121. http://dx.doi.org/10.1144/SP349.6.

Appel E., Müller R. & Widder R.W. (1991) - Palaeomagnetic results from the Tibetan Sedimentary Series of the Manang area (north central Nepal). Geophysical Journal International, 104, 255-266.

Appel E., Crouzet C. & Schill E. (2012) - Pyrrhotite remagnetizations in the Himalaya: a review. Geol. Soc. London Spec. Publ., 371 (1), 163-180.

Armijo R., Tapponnier P., Mercier J.L. & Tonglin H. (1986) - Quaternary extension in southern Tibet: field observations and tectonic implications. Journal of Geophysical Research, 91, 13803-13872.

Berthe´ , D., Choukroune, P. & Jegouzo, P. (1979) - Orthogneiss, mylonite and non coaxial deformation of granites: the example of the South Armorican Shear Zone. Journal of Structural Geology, 1, 31–42.

Bordet P., Colchen M., Krummenacher D., Le Fort P., Mouterde R. & Remy M. (1971) - Recherches géologiques dans l'Himalaya du Népal: Région de la Thakkhola: Paris, Éditions du Centre National de la Recherche Scientifique, 279.

Brown R.L. & Nazarchuk J.H. (1993) - Annapurna detachment fault in the greater Himalaya of Central Nepal. Geological Society of London, 74, 461-473.

Burchfiel B.C., Chen Z., Hodges K.V., Liu Y., Royden L.H., Changrong D. & Xu, L. (1992) - The South Tibetan Detachment System, Himalayan Orogen: extension contemporaneous with and parallel to shortening in a collisional mountain belt. Geological Society of America Special Paper 269, 1-41.

Burkhard M. (1993) - Calcite twins, their geometry, appearance and significance as stress–strain markers and indicators of tectonic regime: a review. Journal of Structural Geology, 15, 351-368.

Burg J.P. & Chen G.M. (1984) Tectonics and structural zonation of Southern Tibet, China. Nature, 311, 219-223.

Carosi R., Lombardo B., Molli G., Musumeci G. & Pertusati P.C. (1998) - The south Tibetan detachment system in the Rongbuk valley, Everest Region. Deformation features and geological implication. Journal of Asian Earth Sciences, 16, 299-311.

Carosi R., Montomoli C. & Visonà D. (2002) - Is there any detachment in the Lower Dolpo (Western Nepal)? Comptes Rendus Geosciences, 334, 933–940.

Carosi R., Montomoli C. & Visonà D. (2007) - A structural transect in the Lower Dolpo: insights on the tectonic evolution of Western Nepal. Journal of Asian Earth Sciences, 29, 407-423.

Carosi R., Montomoli C., Rubatto D. & Visonà D. (2010) - Late Oligocene high-temperature shear zones in the core of the Higher Himalayan Crystallines (Lower Dolpo, Western Nepal). Tectonics, 29, TC4029.

Carosi R., Montomoli C., Rubatto D. & Visonà D. (2013) - Leucogranite intruding the South Tibetan Detachment in Western Nepal: implications for exhumation models in the Himalayas. Terra Nova, 25, 478- 489.

Carosi .R., Montomoli C., Langone A., Turina A., Cesare B., Iaccarino S., Fascioli L., Visonà D., Ronchi A., & Rai S.M. (2015) – Eocene partial melting recorded in peritectic garnets from kyanite-gneiss, Greater Himalayan Sequence, central Nepal. In: "Tectonics of Himalayas" (Editors: S. Mukherjie, R. Carosi, B. Mukherjie, P.van Der Beck, D. Robinson), Geol. Soc. London Special Publication, n. 412, 111-129, doi:10.1144/SP412.1

Catlos E.J., Dubey C.S., Harrison T.M. & Edwards M.A. (2004) - Late Miocene movement within the Himalayan Main Central Thrust shear zone, Sikkim, north-east India. Journal of Metamorphic Geology, 22, 207-226.

Chang C. (1984) - Les caractéristiques tectoniques et l'evolution de la zone de suture du Yarlung-Zangbo. In: Mercier, J. L. & Li, G. C. (eds) Mission Franco-Chinoise Au Tibet 1980: É tude Géologique Et Géophysique De La Croûte Terrestre Et Du Manteau Supérieur Du Tibet Et De L'Himalaya. Editions du Centre National de la Recherche Scientifique, Paris, France, 341–350.

Choukroune P., Rouce F., Pinet B. & Ecors Pyrenees Team (1990) – Main results of the ECORS Pyrenees profile. Tectonophysics, 173, 411–423.

Colchen M., Le Fort P. & Pêcher, A. (1986) - Notice explicative de la carte géologique Annapurna–Manaslu–Ganesh (Himalaya du Népal) au 1:200000e (bilingual: French–English), CNRS, Paris, 1986.

Coleman M.E. (1998) - U-Pb constraints on Oligocene Miocene deformation and anatexis within the Central Himalaya, Marsyandi valley, Nepal. American Journal of Science, 298, 553-571.

Connolly J.A.D. (2005) - Computation of phase equilibria by linear programming: A tool for geodynamic modeling and its application to subduction zone decarbonation. Earth and Planetary Science Letters, 236, 524-541.

Cottle J.M., Waters D.J., Riley D., Beyssac O. & Jessup M.J. (2011) - Metamorphic history of the South Tibetan Detachment System, Mt. Everest region, revealed by RSCM thermometry and phase equilibria modeling. Journal of Metamorphic Geology, 29, 561-582.

Corrie S.L., Kohn M.J., McQuarrie N. & Long S.P. (2012) - Flattening the Bhutan Himalaya. Earth and Planetary Science Letters, 349-350, 67-74.

Crouzet C., Dunkl I., Paudel L., Arkai P., Rainer T.M., Balogh K. & Appel E. (2007) - Temperature and age constraints on the metamorphism of the Tethyan Himalaya in Central Nepal: a multidisciplinary approach. Journal of Asian Earth Sciences, 30, 113-130.

Crouzet C., Stang H., Appel E., Schill E. & Gautam P. (2001) - Detailed analysis of successive pTRMs carried by pyrrhotite in Himalayan metacarbonates: an example from Hidden Valley Central Nepal. Geophysical Journal International, 146, 607-618.

DeCelles P.G., Gehrels G.E., Quade J., Ojha T.P., Kapp P.A. & Upreti, B.N. (1998) - Neogene foreland basin deposits, erosional unroofing, and the kinematic history of the Himalayan fold-thrust belt, western Nepal. Geological Society of America Bulletin, 110, 2–21.

de Sigoyer J., Chavagnac V., Blichert-Toft J., Villa I.M., Luais B., Guillot S., Cosca M. & Mascale G. (2000) - Dating the Indian continental subduction and collisional thickening in the northwest Himalaya: Multichronology of the Tso Morari eclogites. Geology, 28, 487–490.

Dewey J.F. & Bird J.M. (1970) - Mountain belts and the new global tectonics. Journal of Geophysical Research, 75, 2625-2647.

Durney D.W. & Ramsay J.G. (1973) - Incremental strains measured by syntectonic crystal growths. In: de Jong, K.A., Scholten, R. (Eds.), Gravity and Tectonics. Wiley, New York, pp. 67 – 96.

Dupuis C, Hebert R., Dubois-Coté V., Wang C.S., Li Y.L. & Li Z.J. (2006) - Petrology and geochemistry of mafic rocks from mélange and fysch units adjacent to the Yarlung Zangbo Suture Zone, southern Tibet. Chemical Geology, 214, 287-308.

Dunkl I., Antolín B., Wemmer K., Rantitsch G., Kienast M., Montomoli C., Ding L., Carosi R., Appel E., El Bay R., Xu Q. & von Eynatten H. (2011) - Metamorphic evolution of the Tethyan Himalayan flysch in SE Tibet. In: Gloaguen, R., Ratschbacher, L. (Eds.), Growth and Collapse of the Tibetan Plateau. Geological Society of London Special Publications, 353, 45–69.

Franceschelli M., & Memmi I. (1999) - Zoning of chloritoid from kyanite-facies metapsammites, Alpi Apuane, Italy. Mineralogical Magazine, 63, 105-110.

Frank W., Gansser A. & Trommsdorff V. (1977) - Geological observations in the Ladakh area (Himalayas) - A preliminary report. Schweizerische Mineralogische und Petrographische Mitteilungen, 57, 89-133.

Fry N. (1979) - Random point distributions and strain measurement in rocks. Tectonophysics 60, 89-105.

Fuchs G. (1967) - Zum Bau Des Himalaya. Osterreichische Akademie der Wissenschaften, Mathematisch-Naturwissenschafliche Klasse, Denkschriften, 113, 1–211.

Gaetani M. & Garzanti E. (1991) - Multicyclic history of the northern India continental margin (Northwestern Himalaya). American Association of Petroleum Geologist Bulletin, 75, 1427-1446.

Garzanti E. (1999) - Stratigraphy and sedimentary history of the Nepal Tethys Himalaya passive margin. Journal of Asian Earth Sciences, 17, 805-827.

Garzanti E, Girza M., Martellini L. & Nicora A. (1994) - Transition from diagenesis to metamorphism in the Paleozoic to Mesozoic succession of the Dolpo-Manang Synclinorium and Thakkhola Graben (Nepal Tethys Himalaya). Eclogae Geologicae Helvetiae, 87, 613-632.

Gansser A. (1964) - Geology of the Himalayas. Wiley Interscience, London.

Gansser A. (1980) - The significance of the Himalayan suture zone. Tectonophysics, 62, 37-52.

Genier F. & Epard J.L. (2007) - The Fry method applied to an augen orthogneiss: problems and results. Journal of Structural Geology, 29, 209-224.

Godin L., Brown R.L., Hanmer S. & Parrish R. (1999) - Back folds in the core of the Himalayan orogen: An alternative interpretation. Geology, 27, 151-154.

Godin L. (2003) - Structural evolution of the Tethyan sedimentary sequence in the Annapurna area, central Nepal Himalaya. Journal of Asian Earth Sciences, 22, 307-328.

Godin L., Yakymchuk C. & Harris L.B. (2011) - Himalayan hinterland-verging superstructure folds related to foreland-directed infrastructure ductile flow: Insights from centrifuge analogue modelling. Journal of Structural Geology, 33, 329-342

Govindaraju K. (1994) - 1994 compilation of working values and sample description for 383 geostandards. Geostandards Newsletter, 18, 1-158.

Guillot S., Garzanti E., Baratoux D., Marquer D., Maheo G. & de Sigoyer J. (2003) - Reconstructing the total shortening history of the NW Himalaya: Geochemistry, Geophysics, Geosystems, 4.

Harrison T.M., Yin A., Grove M. & Lovera O.M. (2000) - The Zedong Window: A record of superposed Tertiary convergence in southeastern Tibet. Journal of Geophysical Research, 105, 19211-19320.

Heim A. & Gansser A. (1939) - Central Himalaya - Geological observations of Swiss expedition, 1936, Mémoire Société Helvetique Science Naturelle, 73, 1-245.

Herron M.M. (1988) - Geochemical classification of terrigenous sands and shales from core or log data. Journal of Sedimentary Research, 58, 820-829,

Hodges K.V. (2000) - Tectonic of Himalaya and southern Tibet from two perspectives. Geological Society of America Bulletin, 112, 324-350.

Holland T.J.B. & Powell R. (1991) - A compensated-Redlich-Kwong (CORK) equation for volumes and fugacities of CO2 and H2O in the range 1 bar to 50 kbar and 100–1600°C. Contributions to Mineralogy and Petrology, 109, 265-273.

Holland T.J.B. & Powell, R. (1998) - An internally consistent thermodynamic data set for phases of petrological interest. Journal of Metamorphic Geology, 16, 309-343.

Jessup M.J., Cottle M.J., Searle M.P., Law R.D., Newell D.L., Tracy R.J. & Waters D.J. (2008) - P–T–t–D paths of Everest Series schist, Nepal. Journal of Metamorphic Geology, 26, 717-739.

Kellett D.A. & Godin L. (2009) - Pre-Miocene deformation of the Himalayan superstructure, Hidden valley, central Nepal. Journal of Geological Society, 166, 261-275.

Kellett D.A., Grujic D. & Erdmann S. (2009) - Miocene structural reorganization of the South Tibetan detachment, eastern Himalaya: implications for continental collision. Lithosphere, 1, 259-281, doi:10.1130/L56.1.

Hou Z., Zheng Y., Zeng L., Gao L., Li W., Li Q., Fu Q., Liang W. & Sun Q. (2012)- Eocene-Oligocene granitoids in southern Tibet: constraints on crustal anatexis and tectonic evolution of the Himalayan orogen. Earth and Planetary Science Letters, 349-350, 38-52.

Iaccarino S., Montomoli C., Carosi R, Massonne H.J, Langone A. & Visonà D. (2015) - Pressure-temperature-time-deformation path of kyanite-bearing migmatitic paragneiss in the Kali Gandaki valley (Central Nepal): Investigation of Late Eocene-Early Oligocene melting processes. Lithos, 231, 103-121.

Lee J., Hacker B.R., Dinklage W.S., Wang Y., Gans P., Calvert A., Wan J., Chen W., Blythe A.E. & McCelland W. (2000) - Evolution of the Kangmar dome, southern Tibet: Structural, petrologic, and thermochronologic constraints. Tectonics, 19, 872–895.

Leech M.L., Singh S., Jain A.K., Klemperer S.L. & Manickavasagam R.M. (2005) - The onset of India-Asia continental collision: early steep subduction required by the timing of UHP metamorphism in the western Himalaya. Earth and Planetary Science Letters, 234, 83-97.

Le Fort P. (1975) - Himalaya: the collided range. American Journal of Science, 275, 1-44.

Li G, Tian Y., Kohn B.P., Sandiford M, Xu Z. & Cai Z (2015) - Cenozoic low temperature cooling history of the Northern Tethyan Himalaya in Zedang, SE Tibet and its implications. Tectonophysics, 643, 80-93.

Lisle R.J. (1992) - Strain estimation from flattened buckle folds. Journal of Structural Geology, 369–371.

Liu, G. & Einsele, G. (1994) - Sedimentary history of the Tethyan basin in the Tibetan Himalayas. Geologische Rundschau, 83, 32–61.

Lo Pò, D. & Braga R., (2014) - Influence of ferric iron on phase equilibria in greenschist facies assemblages: the hematite-rich metasedimentary rocks from the Monti Pisani (Northern Apennines). Journal of Metamorphic Geology, 32, 371-387.

Massonne H.-J. (2012) -Formation of amphibole and clinozoisite-epidote in eclogite owing to fluid infiltration during exhumation in a subduction channel. Journal of Petrology, 53, 1969-1922, doi: 10.1093/petrology/egs040.

Mercier J.L. *et alii* (1984) - La collision Inde-Asie côté Tibet. In: Mercier, J. L. & Li, G. C. (eds) Mission Franco-Chinoise Au Tibet 1980: Étude Géologique Et Géophysique De La Croûte Terrestre Et Du Manteau Supérieur Du Tibet Et De L'Himalaya. Editions du Centre National de la Recherche Scientifique, Paris, France, 29, 341–350.

Molnar P (1984) – Structure and tectonics of the Himalaya: Constraints and Implications of Geophysical Data. Annual Review of Earth and Planetary Sciences, 12, 489-518.

Molnar P. & Tapponnier P. (1977) - The collision between India and Eurasia. Scientific American, 236, 30-42.

Montomoli C., Iaccarino S., Carosi R., Langone A. & Visonà D. (2013) – Tectonometamorphic discontinuities within the Greater Himalayan Sequence in Western Nepal (Central Himalaya): insights on the exhumation of crystalline rocks. Tectonophysics, 608, 1349–1370.

Montomoli C., Carosi R. & Iaccarino S. (2015) – Tectonometamorphic discontinuities in the Greater Himalayan Sequence: a local or a regional feature? Geological Society, London, Special Publications, 412, 25-41, http://dx.doi.org/10.1144/SP412.3

Murphy M.A. & Yin A. (2003) - Structural evolution and sequence of thrusting in the Tethyan fold-thrust belt and Indus-Yalu suture zone, southwest Tibet. Geological Society of America Bulletin, 115, 21–34.

Najman Y., Appel E., Boudagher-Fadel M., Bown P., Carter A., Garzanti, E., Godin L., Han J.T., Liebke U., Oliver G., Parrish R. & Vezzoli G. (2010) - The timing of India-Asia collision: sedimentological, biostratigraphic and paleomagnetic constraints. Journal of Geophysical Research, 115(B12), B12416.

Pan G., Ding J., Yao D. & Wang L. (2004) - Geological Map of Qinghai-Xizang (Tibet) Plateau and Adjacent Areas (1:1,500,000). Chengdu Institute of Geology and Mineral Resources, China Geological Survey. Chengdu Cartographic Publishing House.

Paudel L.P. & Arita K. (2005) - The b-spacing values of white micas and their metamorphic implications in the Lesser Himalaya, central Nepal. Journal of Asian Earth Sciences, 27, 10-24.

Passchier C.W. & Trouw R.A.J. (2005) - Microtectonics, Springer Verlag, 366 pp.

Pourteau A., Bousquet R., Vidal O., Plunder A., Duesterhoeft E., Candan O. & Oberhänsli R. (2014) - Multistage growth of Fe–Mg–carpholite and Fe–Mg–chloritoid, from field evidence to thermodynamic modelling. Contribution to Mineralogy and Petrology, DOI 10.1007/s00410-014-1090-7.

Quidelleur X., Grove M., Lovera O.M., Harrison T.M., Yin A. & Ryerson F.J. (1997) - Thermal evolution and slip history of the Renbu-Zedong thrust, southeastern Tibet. Journal of Geophysical Research, 102, 2659–2679.

Ramsay J.G. (1967) - Folding and fracturing of rocks. New York, McGraw-Hill, 568 p.

Ramsay J. (1980) - The crack-seal mechanism of rock deformation. Nature, 284, 135-139.

Ratschbacher L., Frisch W., Liu G. & Chen C. (1994) - Distributed deformation in southern and western Tibet during and after the India-Asia collision. Journal of Geophysical Research. 99, 19917-19945.

Robinson D.M., De Celles P.G., Garzione C.N., Pearson O.N., Harrison T.M. & Catlos E.J. (2003) - Kinematic model for the Main Central Thrust in Nepal. Geology, 31, 339–362.

Rowley D.B. (1996) - Age of initiation of collision between India and Asia: A review of stratigraphic data. Earth and Planetary Science Letters, 145, 1-13.

Rowley D.B. (1998) - Minimum age of initiation of collision between India and Asia north of Everest based on the subsidence history of the Zhepure Mountain section. Journal of Geology, 106, 229-235.

Schill E., Appel E., Crouzet C., Gautam P., Wehland F. & Staiger M. (2004) - Oroclinal bending v. regional significant clockwise rotations in the Himalayan arc-Constrains from secondary pyrrhotite remanences. In: Sussman, A. J. & Weil, A. B. (eds) Orogenic Curvature: Integrating Paleomagnetic and Structural Analyses. Geological Society of America, Special Paper, 383, 73–85.

Searle M.P. (1983) - Stratigraphy, structure and evolution of the Tibetan Tethys zone in Zanskar and the Indus suture zone in the Ladakh Himalaya. Royal Society of Edimburgh Transactions, Earth Sciences, 73, 203-217.

Searle M.P. (2001) - Dating the Indian continental subduction and collisional thickening in the northwest Himalaya: multichronology of the Tso Morari eclogites: comment and reply. Geology, 29, 191-192.

Searle M.P. (2010) - Low-angle normal faults in the compressional Himalayan orogen; Evidence from the Annapurna-Dhaulagiri Himalaya, Nepal. Geosphere, 6, 296–315.

Searle M.P., Corfield R.I., Stephenson B. & McCarron J. (1997) - Structure of the north Indian continental margin in the Ladakh-Zanskar Himalayas: Implications for the timing of obduction of the Spontang ophiolite, India-Asia collision and deformational events in the Himalaya. Geological Magazine, 134, 297-316.

Searle M.P., Windley B.F., Coward M.P., Cooper D.J.W., Rex A.J., Rex D.C., Li Tingdong, Xiao Xuchang, Jan M.Q., Thakur V.C. & Kumar S. (1987) - The closing of Tethys and the tectonics of the Himalaya. Geological Society of America Bulletin, 98, 678-701.

Schmid S.M., Froitzheim N., Pfiffner O.A., Schönborn G. & Kissling, E. (1996) – Geophysical-geological transect and tectonic evolution of the Swiss-Italian Alps. Tectonics 15,1036-1064.

Spear F.S. (1993) - Metamorphic phase equilibria and pressure–temperature–time paths. Mineralogical Society of America, Monograph Series, Washington, D.C.

Stöcklin J. (1980) - Geology of Nepal and its regional frame. Journal of the Geological Society, London, 137, 1-34.

Teixell A. (1998) – Crustal structure and orogenic material budget in the west-central Pyrenees. Tectonics, 17, 395-406.

Vannay J.-C. & Steck A. (1995) - Tectonic evolution of the High Himalaya in Upper Lahul (NW Himalaya, India). Tectonics, 14, 253-263.

Valdiya K.S. (1980) - Geology of the Kumaun Lesser Himalaya. Wadia Institute of Himalayan Geology, Dehra Dun.

Vidal O., Goffé B., Bousquet R. & Parra T. (1999) - Calibration and testing of an empirical chloritoid-chlorite Mg-Fe exchange thermometer and thermodynamic data for daphnite. Journal of Metamorphic Geology, 17, 25-39.

Visonà D., Carosi R., Montomoli C., Peruzzo L. & Tiepolo M. (2012) - Miocene andalusite leucogranite in central-east Himalaya (Everest–Masang Kang area): low-pressure melting during heating. Lithos, 144, 194-208.

Vollmer F.W., 2015. EllipseFit 3.2.0. http://www.frederickvollmer.com/ellipsefit/.

Webb A. G., Yin A. & Dubey C.S., (2013) - U-Pb zircon geochronology of major lithologic units in the eastern Himalaya: Implications for the origin and assembly of Himalayan rocks. Geological Society of America Bulletin,125, 499–522; doi: 10.1130/B30626.1.

Wiesmayr G. & Grasemann B. (2002) - Eohimalayan fold and thrust belt: Implications for the geodynamic evolution of the NW-Himalaya (India). Tectonics, 21, 1058, doi:10.1029/2002TC001363, 2002

Whitney D.L. & Evans B.W. (2010) - Abbreviations for names of rock-forming minerals. American Mineralogist, 95, 185-187.

Willner A.P., Sepúlveda F.A., Hervé F., Massonne H.-J. & Sudo M. (2009) - Conditions and timing of pumpellyite-actinolite facies metamorphism in the Early Mesozoic frontal accretionary prism of the Madre de Dios Archipelago (50°20'S; southern Chile). Journal of Petrology, 50, 2127-2155.

Wu C., Nelson K.D., Wortman G., Samson, S.D., Yongiun Y., Jixiang L., Kidd W.S.F. & Edwards M.A. (1998) - Yadong cross structure and South Tibetan detachment in the east central Himalaya (89°-90°E). Tectonics, 17, 28-45, doi: 10.1029/97TC03386.

Xu X., Ding L., Qiang X., Fulong C., Qinghai Z., Liyun Z. & Qingzhou L. (2009) - Tectonic implications of the Ultramafic Dykes in Southeastern Tibet. Chinese Journal of Geology, 44, 1012–1024.

Yan D.P., Zhou M.F., Robinson P.T., Grujic D., Malpasa J., Kennedy A. & Reynolds P. (2012) – Constraining the mid-crustal channel flow beneath the Tibetan Plateau: data from the Nielaxiongbo gneiss dome, SE Tibet. International Geology Review, 54, 6, 615-632.

Yin A. (2006) - Cenozoic tectonic evolution of the Himalayan orogen as constrained by along-strike variation of structural geometry, exhumation history, and foreland sedimentation: Earth-Science Reviews, 76, 1-131.

Yin A., Harrison T.M., Ryerson F.J., Wenji C., Kidd W. & Copeland P. (1994) - Tertiary structural evolution of the Gangdese thrust system, southeastern Tibet. Journal of Geophysical Research, 99, 18,175-18, 201.

Yin A., Harrison T.M., Murphy M.A., Grove M., Nie S., Ryerson F.J., Wang X.F., Chen Z.L. (1999) - Tertiary deformation history of southeastern and southwestern Tibet duringthe Indo-Asian collision. Geological Society of America Bulletin, 111, 1–21.

Zhang B., Zhang J., Guo L. & Wang W. (2005) - Microstructural and deformational studies on mylonite in the detachment faults of Yalashangbo dome, North Himalayan domes zone. Progress in Natural Science, 15, 1005–1013.

Zhang J., Santosh M., Wang X., Guo L., Yang X. & Zhang B. (2012) – Tectonics of the northern Himalaya since the India – Asia collision. Gondwana Research, 21, 939-960.

Zeng L., Gao L., Xie K. & Zeng. (2011) – Mid-Eocene high Sr/Y granites in the Northern Himalayan gneiss dome: melting thickened lower continental crust. Earth and Planetary Science Letters, 303, 251-266

Zhu D., Mo X., Pan G., Zhao Z., Dong G., Shi Y., Liao Z., Wang L. & Zhou C, (2008) -. Petrogenesis of the earliest Early Cretaceous mafic rocks from the Cona area of the eastern Tethyan Himalaya in south Tibet: interaction between the incubating Kerguelen plume and the eastern Greater India lithosphere? Lithos, 100, 147-173.

LIST OF FIGURE AND FIGURE CAPTIONS

Fig. 1 – Schematic geological map modified after Antolin *et alii* (2010 and references therein) where the two main structural domains are shown. In the insets structural projections (Wulff net, lower hemisphere) of the main structural elements are shown. Abbreviations: TSS: Tethyan Sedimentary Sequence; GHS = Greater Himalayan Sequence; NHGD: North Himalayan Gneiss Dome; LB = Lhasa Block; STDS = South Tibetan Detachment System; GCT = Great Counter Thrust. . Red line: trace of geological cross section

Fig. 2 – Main outcrop's features along a S-N structural transect. a) Southward facing decametric F1 tight fold. In the insert load cast structures from the upper limb of fold pointing out normal polarity of bedding; b) Calcitic strain fringes around pyrite crystal; c) Northward verging F2 fold; d) Brittle – ductile shear zones with well developed C-S fabric pointing out a top-to-the-NE sense of shear. See text for more explanations.

Fig. 3 – Microscopic aspect of S1, S2 and S3 foliations moving from S to N: a) Fine continuous S1 foliation deformed by a faible S2 crenulation cleavage in the southern portion of domain 1; b) S2 Spaced foliation with dynamic recrystallization (central portion of the transect). In the microlithons S1 is preserved; c) fine continuous transpositive S2 foliation with dynamic recrystallization (Northernmost portion of the transect); d) Microscopic features of S3 gradational crenulation cleavage. No dynamic recristallization has been observed. S1 and S2 foliations are also present.

Fig. 4: Example of strain analyses on F2 fold profile according to Lisle's method (1992) (CM11 fold). Left: redrawn fold profile along which measurements of orthogonal thickness (t1, t2, t3..) of folded layers have been taken at different dipping angles (1, 2, 3,…); Right: Construction of

strain ellipse plotting inverse thicknesses at different dipping angles (Inverse thickness measurements have been plotted at 1:5 scale for graphical resolution of strain ellipse).

Fig. 5: a) Microphotograph of metarenites used for strain analyses (sample CM4). Quartz pebbles have been used as strain markers (Crossed nicols); b) example of finite strain calculation using Ellipse fit program (Vollmer, F.W., 2015. EllipseFit 3.2.0. http://www.frederickvollmer.com/ellipsefit) (N= number of centers, R= estimated strain ratio; a: orientation of the strain ellipse long axes respect to a horizontal reference line)

Fig. 6: Microstructural aspects of sample WE-09. (a) General view of the sample, showing the three main foliations (S1, S2, S3); (b) relationship between main foliation (S2), and Cld porphyroblast internal foliation (Si). The Si is continuous with the external S2 foliation; (c) decussate Cld porphyroblast; (d) close up view of Cld dissolution along S3 surface (arrow);

Fig. 7: Chemical composition of main minerals: (a) XMg Cld vs MnO (wt%) showing Cld zoning. In the inset qualitative (SEM based) Fe X-ray map of Cld porphyroblast shows Fe-rich core and Fe-poor rim; (b) Compositions of Wm. The line represents ideal muscovite-(Fe,Mg) aluminoceladonite join;

Fig. 8: (a) P-T pseudosection for sample WE-09; (b) Si (p.f.u.) isopleths in Wm (c) Isopleths of XMg in Cld.

Fig. 9: Inferred P-T path for Cld-bearing WE-09 sample based on P-T pseudosection and chlorite-chloritoid thermometer ($T_{V\&al99}$) of VIDAL *et alii* (1999)

LIST OF TABLES

Table 1: Rxz finite strain data from metarenites applying Fry and Ramsay's methods (Method 1: FRY, 1969, Method 2: RAMSAY, 1967) and from Lisle's method (Method 3: LISLE, 1992) on selected F2 folds along a S-N transect. See text for more details.

Table 2 : representative mineral chemistry of Cld, Chl and Wm. Abbreviations as follows: C= core, R= rim, S1= foliation in the microlithons, S2=main foliation, nor.O= normalized oxygens.

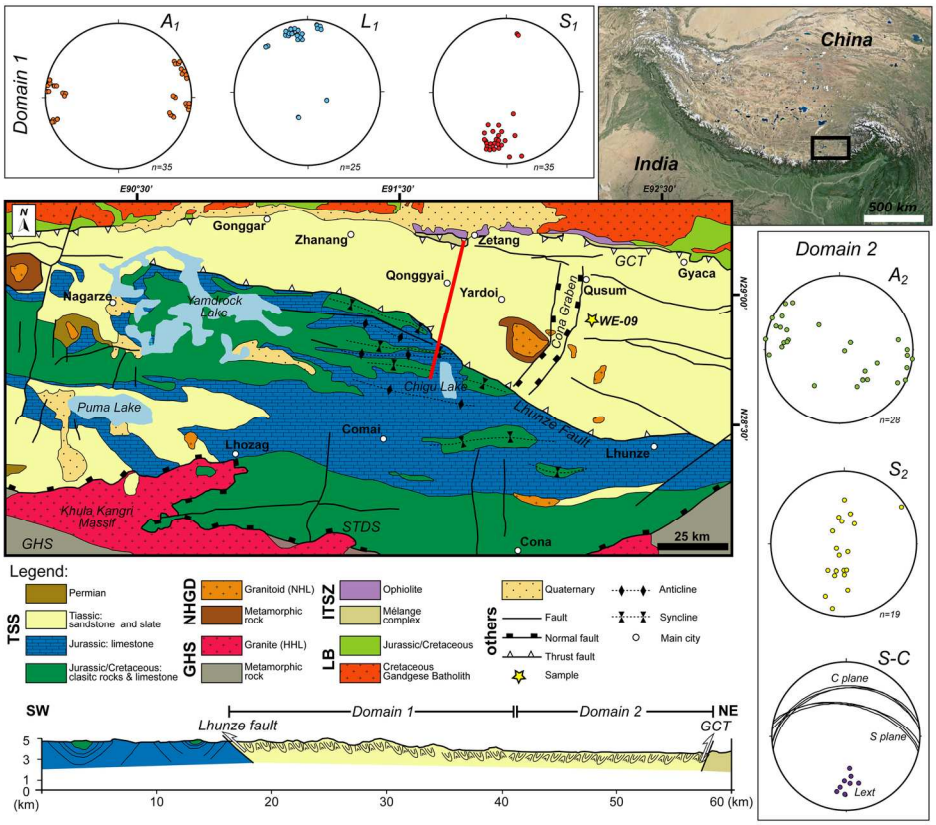

Fig. 1 – Schematic geological map modified after Antolin et alii (2010 and references therein) where the two main structural domains are shown. In the insets structural projections (Wulff net, lower hemisphere) of the main structural elements are shown. Abbreviations: TSS: Tethyan Sedimentary Sequence; GHS = Greater Himalayan Sequence; NHGD: North Himalayan Gneiss Dome; LB = Lhasa Block; STDS = South Tibetan Detachment System; GCT = Great Counter Thrust. . Red line: trace of geological cross section
164x136mm (300 x 300 DPI)

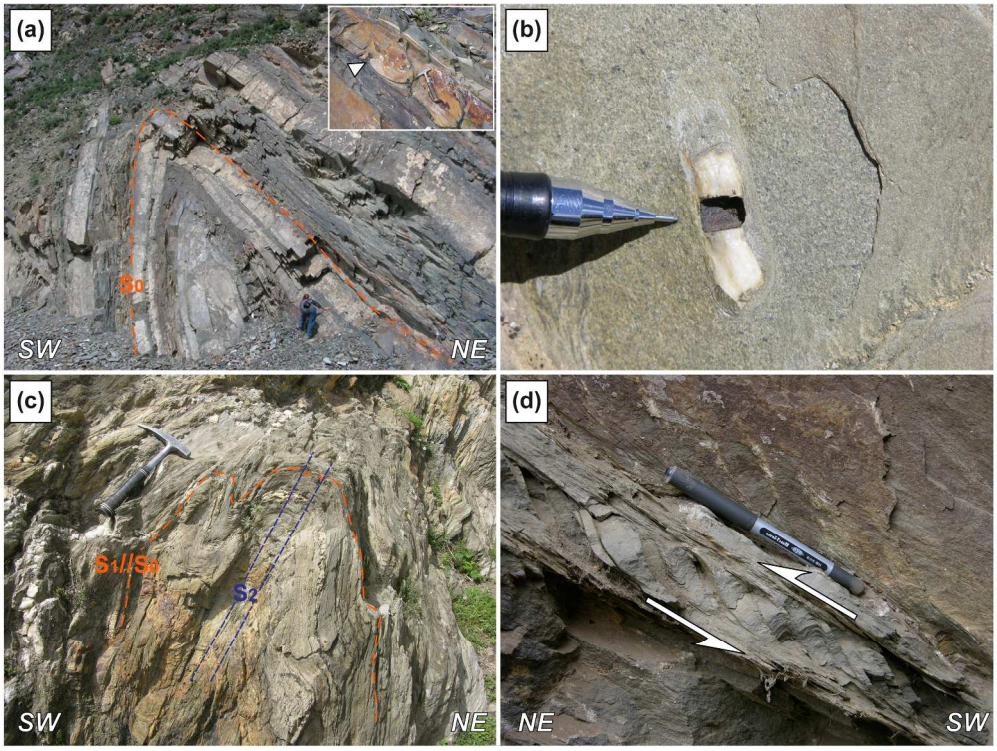

Fig. 2 – Main outcrop's features along a S-N structural transect. a) Southward facing decametric F1 tight fold. In the insert load cast structures from the upper limb of fold pointing out normal polarity of bedding ; b) Calcitic strain fringes around pyrite crystal; c) Northward verging F2 fold; d) Brittle – ductile shear zones with well developed C-S fabric pointing out a top-to-the-NE sense of shear. See text for more explanations. 242x180mm (300 x 300 DPI)

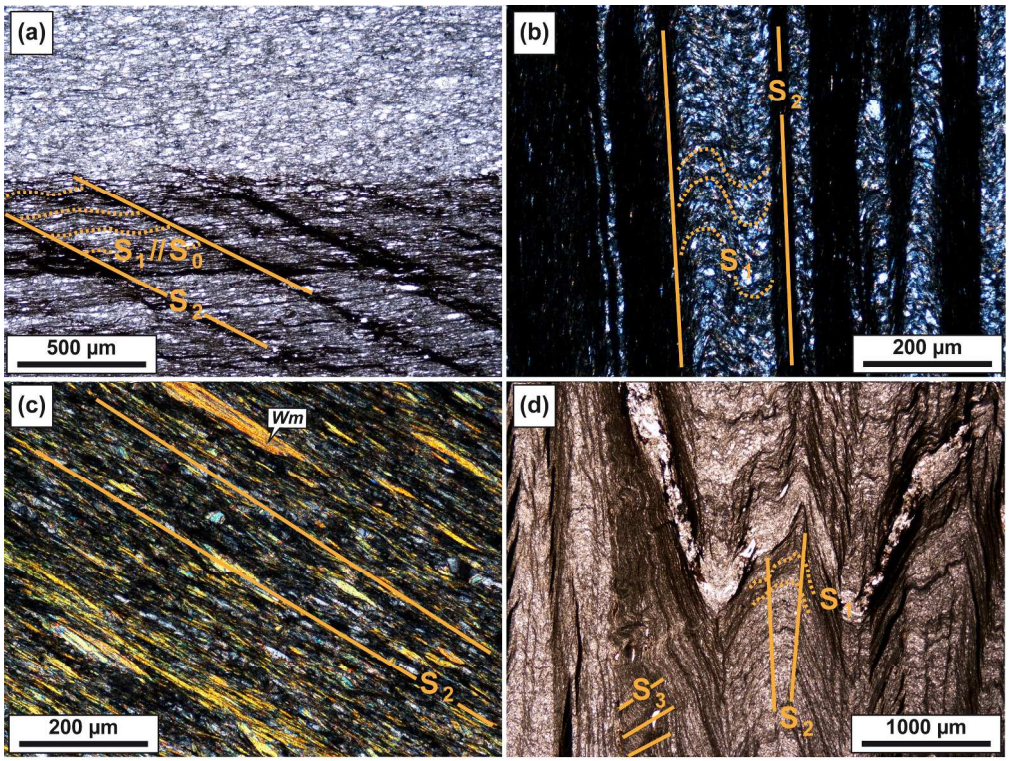

Fig. 3 – Microscopic aspect of S1, S2 and S3 foliations moving from S to N: a) Fine continuous S1 foliation deformed by a faible S2 crenulation cleavage in the southern portion of domain 1; b) S2 Spaced foliation with dynamic recrystallization (central portion of the transect). In the microlithons S1 is preserved; c) fine continuous transpositive S2 foliation with dynamic recrystallization (Northernmost portion of the transect); d) Microscopic features of S3 gradational crenulation cleavage. No dynamic recristallization has been observed. S1 and S2 foliations are also present.
241x181mm (300 x 300 DPI)

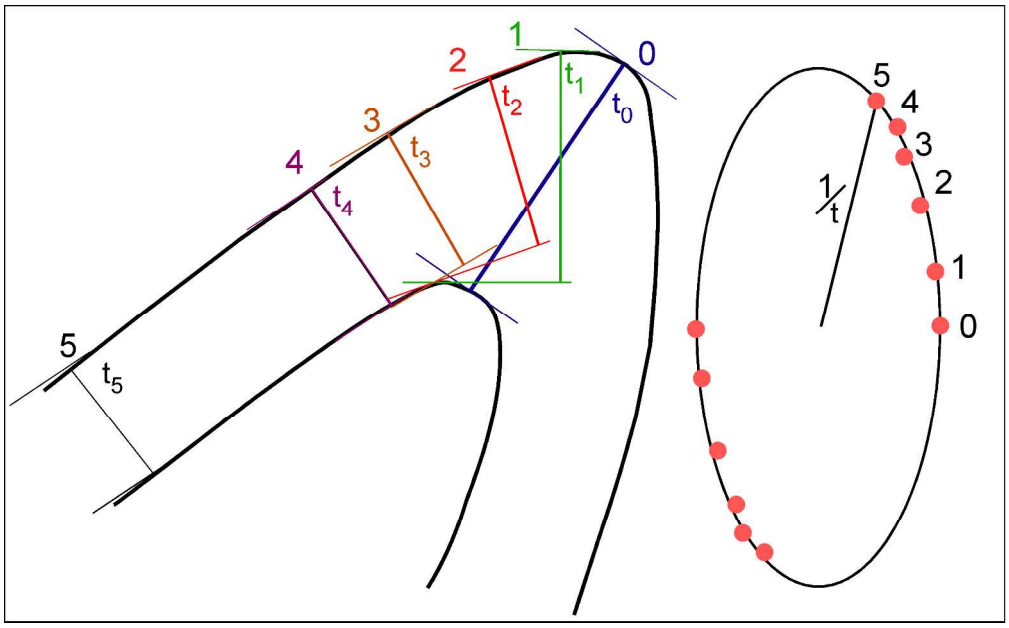

Fig. 4: Example of strain analyses on F2 fold profile according to Lisle's method (1992) (CM11 fold). Left: redrawn fold profile along which measurements of orthogonal thickness (t1, t2, t3..) of folded layers have been taken at different dipping angles (1, 2, 3,…); Right: Construction of strain ellipse plotting inverse thicknesses at different dipping angles (Inverse thickness measurements have been plotted at 1:5 scale for graphical resolution of strain ellipse).

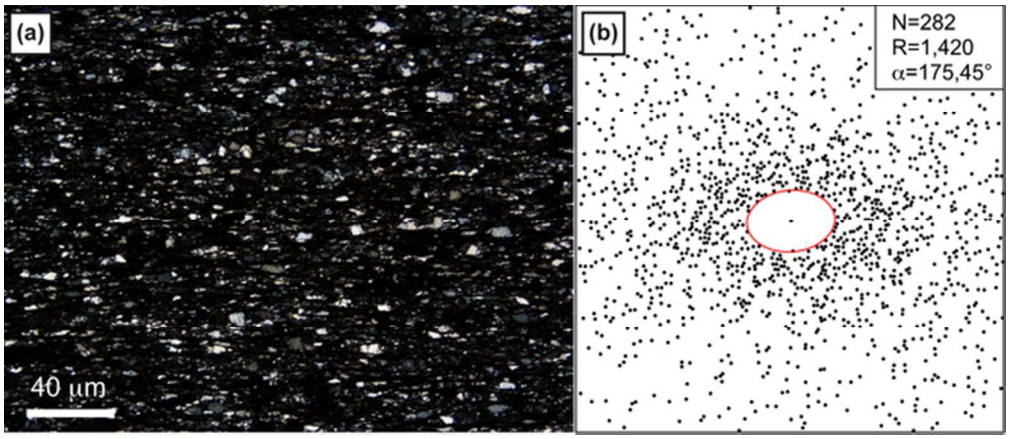

Fig. 5: a) Microphotograph of metarenites used for strain analyses (sample CM4). Quartz pebbles have been used as strain markers (Crossed nicols); b) example of finite strain calculation using Ellipse fit program (Vollmer, F.W., 2015. EllipseFit 3.2.0. http://www.frederickvollmer.com/ellipsefit/) (N= number of centers, R= estimated strain ratio; a: orientation of the strain ellipse long axes respect to a horizontal reference line) 56x24mm (300 x 300 DPI)

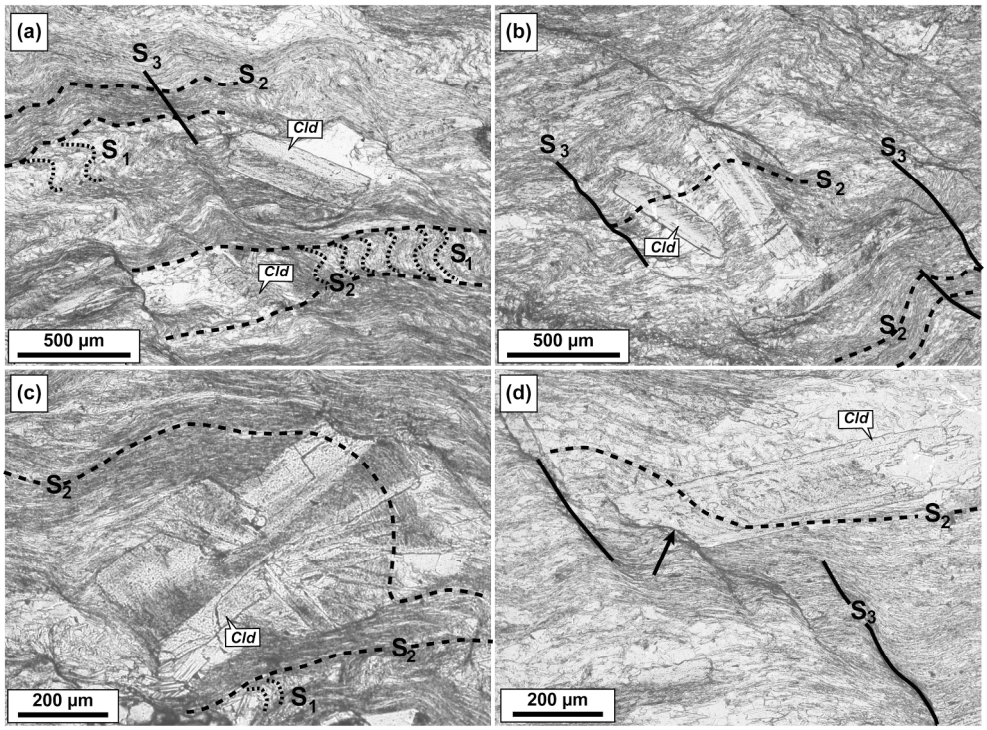

Fig. 6: Microstructural aspects of sample WE-09. (a) General view of the sample, showing the three main foliations (S1, S2, S3); (b) relationship between main foliation (S2), and Cld porphyroblast internal foliation (Si). The Si is continuous with the external S2 foliation; (c) decussate Cld porphyroblast; (d) close up view of Cld dissolution along S3 surface (arrow);
250x190mm (300 x 300 DPI)

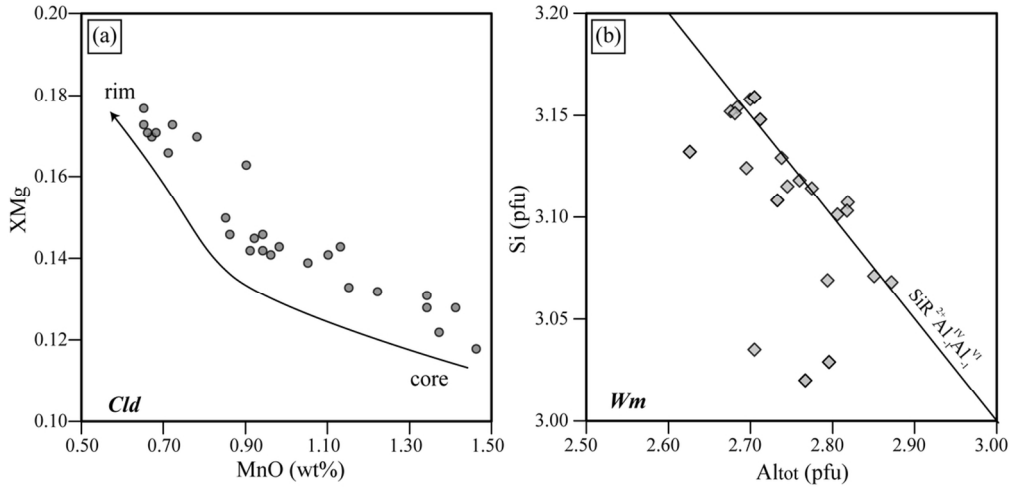

Fig. 7: Chemical composition of main minerals: (a) XMg Cld vs MnO (wt%) showing Cld core-rim zoning; (b) Compositions of Wm. The line represents ideal muscovite-(Fe,Mg) aluminoceladonite join;
106x51mm (300 x 300 DPI)

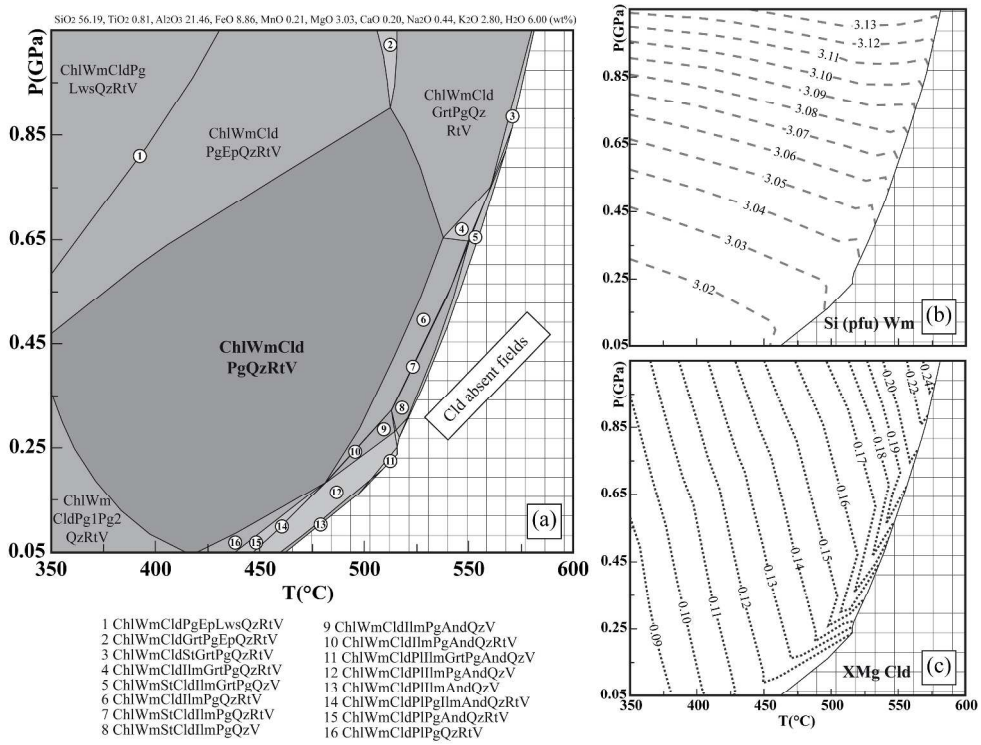

Fig. 8: (a) P-T pseudosection for sample WE-09; (b) Si (p.f.u.) isopleths in Wm (c) Isopleths of XMg in Cld. 327x256mm (300 x 300 DPI)

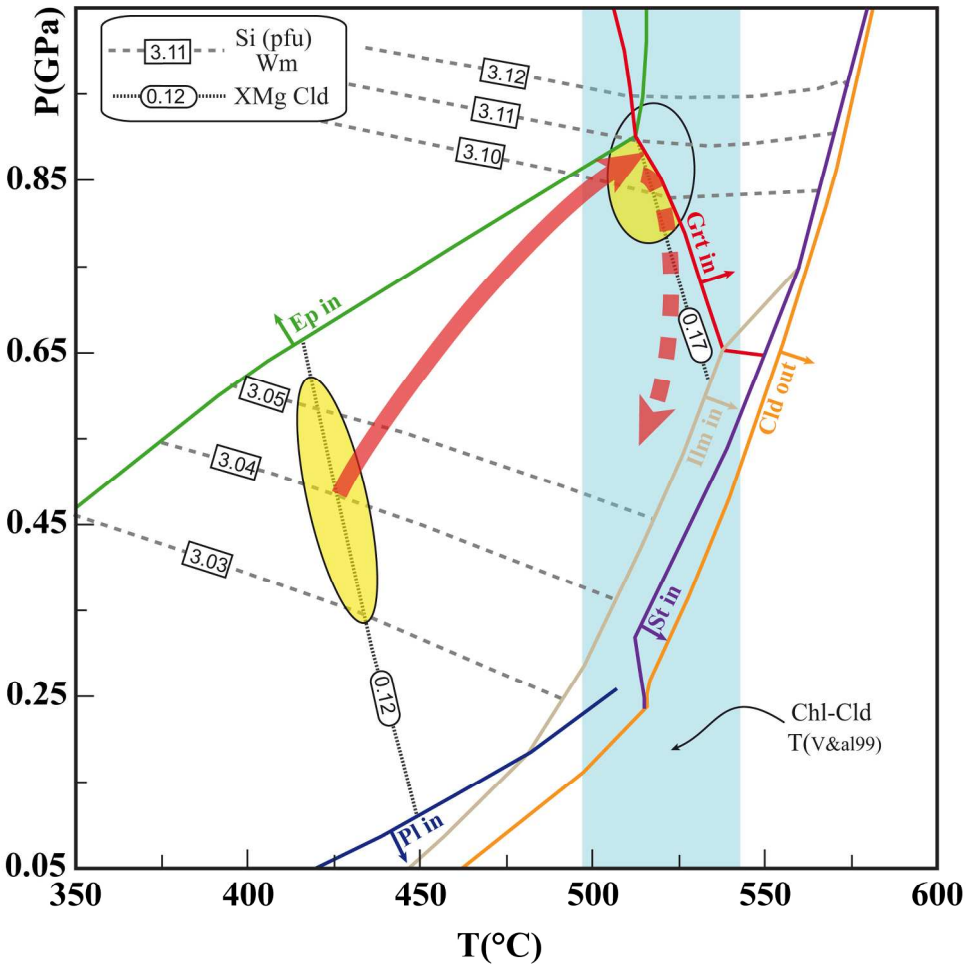

Fig. 9: Inferred P-T path for Cld-bearing WE-09 sample based on P-T pseudosection and chlorite-chloritoid thermometer (TV&al99) of VIDAL et alii (1999)
198x199mm (300 x 300 DPI)

Sample	Method 1		Method 2			*Sample*	Method 3	*South*
	n° centers	Rxz	Rfmax	Rf min	Rxz		Rxz	
CM1	191	1.234	3.0	1.43	2.07	*CM7*	1.06	
CM2	91	1.251	3.14	1.40	2.09	*CM8*	1.26	
CM3	98	1.273	3.67	1.40	2.26	*CM9*	1.45	
CM4	282	1.420	4.00	1.44	2.40	*CM10*	2.04	
CM5	96	1.484	4.29	1.50	2.53	*CM11*	2.26	
CM6	119	1.488	4.44	1.60	2.66			*North*

Table 1: Rxz finite strain data from metarenites applying Fry and Ramsay's methods (Method 1: FRY, 1969, Method 2: RAMSAY, 1967) and from Lisle's method (Method 3: LISLE, 1992) on selected F2 folds along a S-N transect. See text for more details.

Table 2: Representative mineral chemistry of Cld, Chl and Wm.
Abbreviations as follows: C = core, R = rim, S1 = foliation in the microlithons, S2= main foliation, nor. O = normalized oxygens.

	Cld (C)	Cld (R)	Cld (C)	Cld (R)	Chl	Chl	Chl	Chl	Wm (S1)	Wm (S1)	Wm (S2)	Wm (S2)
SiO_2	24.44	24.65	25.99	24.02	24.42	24.34	24.59	25.11	44.64	45.58	46.78	46.86
TiO_2	0.04	0.03	0.02	0.01	0.05	0.05	0.12	0.15	0.18	0.25	0.19	0.23
Al_2O_3	40.92	41.18	39.81	41.35	24.05	23.98	24.12	24.44	34.69	35.19	33.98	34.95
Cr_2O_3	0.00	0.02	0.05	0.01	0.02	0.00	0.04	0.04	0.03	0.04	0.00	0.04
Fe_2O_3*	0.00	0.00	0.00	0.32	0.00	0.00	0.00	0.00	2.27	1.51	0.00	1.40
FeO	24.39	23.48	23.86	23.00	25.18	25.33	25.08	24.39	0.88	0.58	1.14	0.54
MnO	1.46	0.78	1.37	0.65	0.27	0.32	0.32	0.37	0.06	0.03	0,02	0.00
MgO	1.82	2.70	1.87	2.77	13.90	13.83	12.53	10.95	1.59	0.65	1.06	1.09
CaO	0.01	0.01	0.01	0.01	0.02	0.01	0.00	0.03	0.06	0.03	0.00	0.03
Na_2O	0.02	0.00	0.00	0.02	0.02	0.00	0.06	0.17	1.08	1.07	0.89	0.87
K_2O	0.00	0.04	0.02	0.01	0.00	0.01	0.19	0.46	7.54	8.27	8.71	8.51
Total	93.10	92.89	93.00	92.17	87.93	87.87	87.06	86.10	93.02	93.21	92.77	94.51
nor. O	6	6	6	6	14	14	14	14	11	11	11	11
Si	1.007	1.009	1.065	0.990	2.561	2.557	2.680	2.679	3.020	3.069	3.159	3.108
Ti	0.001	0.001	0.001	0.000	0.004	0.004	0.007	0.012	0.009	0.013	0.009	0.011
Al	1,987	1.988	1.924	2.010	2.973	2.970	3.031	3.074	2.767	2.794	2.705	2.733
Cr	0.000	0.001	0.002	0.000	0.002	0.000	0.003	0.004	0.001	0.002	0.000	0.002
Fe^{3+}	0.000	0.000	0.000	0.010	0.000	0.000	0.000	0.000	0.116	0.077	0.000	0.070
Fe	0.840	0.804	0.818	0.793	2.208	2.226	2.131	2.176	0.050	0.033	0.064	0.030
Mn	0.051	0.027	0.048	0.023	0.024	0.028	0.030	0.033	0.003	0.002	0.001	0.000
Mg	0.112	0.165	0.114	0.170	2.172	2.166	1.877	1.741	0.161	0.066	0.107	0.107
Ca	0.000	0.000	0.000	0.000	0.002	0.001	0.004	0.003	0.004	0.002	0.000	0.002
Na	0.002	0.000	0.000	0.002	0.004	0.000	0.006	0.036	0.142	0.140	0.117	0.112
K	0.000	0.002	0.001	0.001	0.000	0.001	0.063	0.062	0.651	0.711	0.750	0.720

* Fe_2O_3 as estimated by A-X software